NASA Technical Memorandum 85815

AN EXPERIMENTAL AND THEORETICAL ANALYSIS OF THE AERODYNAMIC CHARACTERISTICS OF A BIPLANE-WINGLET CONFIGURATION

PETER D. GALL

June 1984

National Aeronautics and
Space Administration

Langley Research Center
Hampton, Virginia 23665

SUMMARY

Improving the aerodynamic characteristics of an airplane with respect to maximizing lift and minimizing induced and parasite drag are of primary importance in designing lighter, faster, and more efficient aircraft. Previous research done by Olson (Ref. 18) has shown that a properly designed biplane wing system can perform superiorly to an equivalent monoplane system with regard to maximizing the lift to drag ratio and efficiency factor. Biplanes offer several advantages over equivalent monoplanes, such as a 60% reduction in weight, greater structural integrity, and increased roll response. The purpose of this research is to examine, both theoretically and experimentally, the possibility of further improving the aerodynamic characteristics of the biplane configuration by adding winglets. Theoretical predictions were carried out utilizing vortex-lattice theory, which is a numerical method based on potential flow theory. Experimental data were obtained by testing a model in the Pennsylvania State University's subsonic wind-tunnel at a Reynolds number of 510,000. Results indicate that the theoretical predictions agree fairly well with the experimental results. More importantly, the results showed that the addition of winglets improved the performance of the biplane with respect to increasing the lift-curve slope, increasing the maximum lift coefficient, increasing the efficiency factor, and decreasing the induced drag.

Page intentionally left blank

LIST OF SYMBOLS

AR	aspect ratio
b	wing span
C_D	total drag coefficient
C_{D_i}	induced drag coefficient
$C_{D_{min}}$	minimum profile drag coefficient
ΔC_{D_p}	incremental change in profile drag due to lift
C_L	finite wing lift coefficient
C_ℓ	section lift coefficient
C_{L_α}	finite wing lift-curve slope
c	streamwise chord
D_i	induced drag force
Dec	biplane decalage angle
e	wing efficiency factor
Ga	biplane gap
Fws	downwash influence coefficient for the starboard planform
Fwp	downwash influence coefficient for the port planform
Fvs	sidewash influence coefficient for the starboard planform
Fvp	sidewash influence coefficient for the port planform
i	local deflection of control point located on the winglet
M	one-half the total number of horseshoe vortices located on the horizonal (wing) planform surface
N	one-half the total number of horseshoe vortices located on the entire planform surface
pn, qn, rn	coordinates of a particular horseshoe vortex in the P,Q,R axis system

p_ν, q_ν, r_ν	coordinates of a particular control point in the P,Q,R axis system
S	area of the horizonal (wing) planform surface
s	semi-width of a horseshoe vortex
V_∞	freestream velocity
v	sidewash velocity in the q-direction
w	downwash velocity in the r-direction
x, ys, z	coordinates of a particular control point (located on the starboard planform) relative to a particular horseshoe vortex
x, yp, z	coordinates of a particular control point (located on the port planform) relative to a particular horseshoe vortex
α	local angle of attack of control point located on the horizonal (wing) planform surface
Γ	circulation strength of a horseshoe vortex
ε	wing twist
ρ	mass density of air
ϕ	deflection angle of planform surface in the QR-plan

Subscripts

n	number designating a particular horseshoe vortex
w	wing or horizonal planform surface
w_ℓ	winglet or vertical planform surface
ν	number designating a particular control point

CHAPTER I

INTRODUCTION

In modern times, with the advent of wide-body jets and supersonic transports, the aircraft has proven to be a very fast and efficient means of transportation from a passenger-seat-miles-per-gallon standpoint. However, private, corporate, and business travel in light aircraft, commonly referred to as general aviation, also plays a vital role in America's transportation system. For transportation needs between cities located approximately 100 to 500 miles apart, the light aircraft is a very attractive means of transportation. For example, a small four-place single-engine aircraft, such as a Mooney 201, will transport four people at 187 miles per hour while burning 9.9 gallons of fuel per hour. This translates to 18.9 statute miles traveled per gallon of fuel burned, or 75.6 passenger-seat-miles-per-gallon. This is not as efficient as a small automobile. However, when considering the high speed and straight line travel which the airplane affords, it appears to be quite advantageous. Compare this to a McDonell-Douglas DC-10 wide-body jet, which can transport 255 passengers at a specific range of 0.22 miles traveled per gallon of fuel burned. This yields 56.1 passenger-seat-miles-per-gallon. From this standpoint, it can be seen that the general aviation airplane is the more

efficient means of transportation. However, for the general aviation airplane to remain an efficient means of transportation, continous improvements must be made on improving aerodynamic efficiency and reducing drag. The high cost of aviation fuel, coupled with increasing operating and maintenance costs, is forcing aircraft manufacturers to design and build more efficient and better performing aircraft. The National Aeronautics and Space Administration (NASA) has been performing a great deal of research in the area of improving aerodynamic efficiencies. Such research projects include experimentation with winglets and wing-tip extensions on general aviation aircraft, as well as first and second generation jet transports. It has been determined that properly designed winglets can significantly reduce induced drag at cruise lift coefficients without imposing severe additional structural loads (Ref. 4).

It is the purpose of this research to study, both experimentally and theoretically, the aerodynamic characteristics and aerodynamic efficiencies of a biplane configuration utilizing winglets. In present literature, there is very little material available on the aerodynamic theory of biplanes. In the early days of aviation, when the monoplane was first introduced, research on biplane theory was virtually discontinued. The analytical determination of biplane characteristics was very complicated due to the

complex interactions between the two wings operating in close proximity to each other. Until recently, very few attempts have been made to optimize the aerodynamic efficiency of the biplane.

If a biplane wing system could be designed to operate as efficiently as an equivalent monoplane system (with the same equivalent wing loading and aspect ratio), the biplane would offer several advantages. Because of the decreased structural constraints of the biplane, the biplane wing system can be as much as 60% lighter in weight than the equivalent monoplane system. Also, because of the increased roll response of the biplane, much less aileron area is required. This means that most of the wing's trailing edge can be utilized for high lift devices, such as fowler flaps. Biplanes offer the potential for excellant low-speed maneuverability, good short-field performance, good load carrying capability and rugged construction.

Previous Investigations

There are three terms commonly used to define the geometry of a given biplane configuration. They are gap, stagger, and decalage. The gap(Ga) is the distance one wing is located above the other measured in percent chord length. Stagger(St) is the distance the upper wing is ahead of, positive, or behind, negative, the lower wing measured in percent chord length. Decalage(Dec) is the angle between

the chord lines of the upper and lower wings. The decalage angle is negative when the lower wing is at a greater angle of attack than the upper wing.

In 1918 F.H. Norton (Ref. 17) conducted experiments utilizing three-dimensional non-symmetrical biplane airfoils. His results showed that maximum aerodynamic effiency is achieved at the highest degree of stagger physically possible. He varied only the stagger while holding the decalage constant at 0 degrees and the gap constant at one chord length. Also, Norton discovered that positive stagger greatly reduces the center of pressure travel, which simplifies the problem of stability.

In 1929 Knight and Noyes (Refs. 11-13) conducted several three-dimensional non-symmetrical biplane airfoil tests and concluded that increasing stagger in the positive direction, or increasing the gap, tends to equalize the loads on the two wings (this does not entirely agree with the results predicted theoretically by the vortex-lattice computer program). They also discovered that changes in decalage from 0 degrees for the orthogonal biplane (stagger equal to zero and gap equal to one chord length) tended to reduce the maximum lift coefficient. This is because (for the orthogonal case) the greatest maximum lift coefficient is reached when both wings stall nearly together. This occurs when they are at the same effective angle of attack. If positive stagger is present, the lower wing must be

operating at a higher angle of attack (negative decalage angle) than the upper wing in order to have sufficient stall match. This effect is due to the lower wing being emersed in the downwash of the upper wing, thereby reducing the effective angle of attack of the lower wing.

In 1936 M. Nenadovitch (Ref. 16) conducted several experiments to determine the aerodynamic characteristics of two-dimensional symmetrical biplane airfoils. He discovered that at a gap of one chord length, a stagger of one chord length, and a decalage angle of -6 degrees there was a substantial reduction in drag.

These results are significant. However, in none of the previous experimentation has any comparison been made to an equivalent monoplane configuration until 1974. In 1974 E.C. Olson (Ref. 18) conducted extensive experimentation on three-dimensional non-symmetrical airfoil biplane configurations in which the geometry was varied about Nenadovitch's optimum test configurations. However, in conjunction with the various biplane configuration tests, Olson also tested an equivalent monoplane system. This is a monoplane system which has the same wing area as the biplane system as well as a similarily related aspect ratio. He discovered that at certain optimized geometric configurations, the biplane outperformed the monoplane configuration with respect to minimum drag and maximum lift to drag ratio. The biplane configurations were tested with

and without the fuselage. Specifically, Olson's experiments resulted in the following conclusions:

1. At a gap of one chord length, a stagger of 0.875, and a decalage angle of -6 degrees,the biplane configuration showed a 25% reduction in drag over the monoplane at a typical cruise lift coefficient.

2. At a gap of one chord length, a stagger of 0.875, and a decalage angle of -5 degrees, the biplane configuration showed a 31.2% increase in the maximum lift to drag ratio while producing a 21.4% reduction in drag over the monoplane.

3. The most effective overall biplane configuration was found at a gap of 0.875, a stagger of one chord length, and a decalage angle of -6 degrees. This biplane configuration showed a 16.3% increase in the in the maximum lift to drag ratio, and a 14.3% reduction in drag at a lift coefficient of 0.175.

4. All biplane configurations showed a reduction in the maximum lift coefficient when compared to an equivalent monoplane configuration.

Past research has shown that the addition of winglets to a given wing configuration can significantly reduce the induced drag. The presence of the winglets causes a physical constraint to the flow field near the location of the winglet, which is usually at or near the wing-tip. This constraint weakens the strength of the trailing vortices shed near the vicinity of the wing-tip. This reduction in the strength of the trailing vortices causes a reduction in the induced downwash, particularily in the vicinity of the outboard section of the wing. By reducing the induced

downwash, the effective angle of attack of the wing is increased. This results in a more even spanwise load distribution across the wing; the net result being a more efficient wing.

The geometric configuration of the winglet is primarily described by two parameters: the winglet cant angle and the winglet toe angle. The cant angle is defined as the angular deflection of the winglet planform relative to a vertical plane which is perpendicular to the aircraft's lateral axis. At a cant angle of 90 degrees, the winglet acts as a wing-tip extension, which is unfavorable because of the increased bending stresses imposed on the wing structure. Also, a cant angle of 0 degrees is unfavorable due to the increase in interference drag caused by thickening boundary layer interactions at the wing-winglet joint. The toe angle is the incident angle of attack at which the winglet is mounted relative to the airplane's longitudal axis.

In addition to altering the spanwise load distribution, the winglet can also induce a negative drag contribution. This is caused by the forward tilting of the winglet normal force vector. This forward tilting effect is caused by the winglet operating at an induced angle of attack, which is brought about by the vectorial addition of the sidewash velocity and freestream velocity vectors.

Description of Research

The purpose of this research is to investigate the possibility of further increasing the aerodynamic performance of the biplane configuration by adding winglets to the already optimized biplane configurations found in Olson's experiments. Pertinent aerodynamic characteristics of the biplane-winglet configuration will be predicted theoretically as well as determined experimentally. If the biplane-winglet configuration could be optimized to the extent that it could perform as well as an equivalent monoplane (with respect to minimizing drag and maximizing the lift to drag ratio), the biplane could offer several advantages, which have been previously mentioned.

The first step in this research was to theoretically analyze and predict the aerodynamic performance of a given biplane configuration with and without winglets. The method used was a finite-element, three-dimensional potential flow code , commonly refered to as the vortex-lattice method. Vortex-lattice utilization is commonly used throughout industry and government research to predict subsonic aerodynamic characteristics of complex planforms as well as predicting spanwise and chordwise load distributions on aerodynamic structures. Research has shown vortex-lattice theory to predict aerodynamic characteristics of complex planforms with considerable accuracy.

The second step was to experimentally test an already optimized design configuration. Based on previous research done by Nenadovitch and Olson, it was determined that the optimum test case would be a biplane-winglet configuration with a gap of one chord length, and a stagger of one chord length. The configuration was tested with and without winglets at a Reynolds number of approximately 510,000. The decalage angle was varied from 0 to -5 degrees. The experimental data was then reduced and several wind tunnel correction factors applied to yield experimentally correct lift and drag data.

CHAPTER II

PRESENTATION OF THEORY

Before the advent of modern high-speed computers, simple problems in aerodynamics had to be solved using classical theory. As the problems became more complex, the application of classical theory became quite cumbersome due to the complex conformal transformations which had to be utilized. It was very difficult to optimize a given design except through trial and error. The analytical approach to predicting the aerodynamic characteristics of a relatively simple biplane configuration proved to be quite cumbersome, even for a simple mathmatical model such as the classical bound-vortex lifting-line method. The addition of winglets to the biplane configuration makes the problem much more complex. The interference effects of all components must be considered, since they have a significant effect on the induced drag and spanwise load distribution.

Basically, the vortex-lattice method is a finite-element method which utilizes a vortex-lattice representation of the aircraft's lifting surfaces coupled with classic equations and theorems for computing aerodynamic characteristics such as lift, induced drag, spanwise load distributions, and wing efficiency factors. This method assumes steady, irrotational, inviscid, incompressible, attached flow. Therefore, numerical results

can only be assumed valid at subsonic speeds when the wing system is operating at a less than critical angle of attack. The vortex-lattice method is commonly used for predicting the aerodynamic characteristics of complex three-dimensional planforms such as the Lockheed boxplane and Whitcomb winglet configuration (Ref. 4). In this research, the vortex-lattice method will be utilized in predicting the aerodynamic performance of the biplane-winglet configuration.

Basic Theoretical Concepts

Fundamental to the development of the vortex-lattice model is the representation of the aircraft's non-planer lifting surfaces by a system of rectangular horseshoe vortices. Basically, each planform surface is divided into several finite elemental panels which extend chordwise and spanwise across the entire planform surface. At the quarter chord point of each elemental panel a bound horseshoe vortex is located, and at the three-quarter chord point a corresponding control point is located. Figure 2-1 shows a typical section of wing which has been broken down into several elemental panels. At each control point the no-flow through condition must be satisfied; that is, the flow must be tangential to the planform surface at this point. This concept first appeared in a paper by E. Pistolesi 1937 (Ref. 5). He found that by using the 1/4-3/4 chord

rule, section lift and moment predictions for a cambered airfoil at a constant angle of attack were exactly that of thin-airfoil theory. In 1942 J. Weissinger applied this method to wing configurations of finite aspect ratio and also achieved accurate results. This method has been widely accepted and is used throughout present research which utilizes vortex-lattice methods.

The first step in utilizing vortex-lattice theory, assuming the planform geometry has been defined, is to determine the number of chordwise and spanwise horseshoe vortices that are to be located on the planform surfaces. The three-dimensional coordinates which locate the bound horseshoe vortices are next computed, as well as computing the coordinates of the cooresponding control points. Once this is accomplished, the induced velocities from the total vortex system can be equated to the freestream velocity component normal to the lifting surface at each control point. Application of the tangent flow boundary condition, (assuming a symmetrical loading) will yield a set of N simultanious equations, each equation consisting of N unknown horseshoe vortex strengths. The fundamental laws of induced velocity from a vortex filament are utilized in calculating the horseshoe vortex induced flow-field at each control point. Once the set of N simultanious equations is solved, and the strength of each individual horseshoe vortex is determined, the Kutta-Joukowski theorem for lift from a

vortex filament is utilized to determine the section lift coefficient. Finally, the finite wing lift coefficient can be obtained by numerically integrating the spanwise load distribution across the entire planform surface.

The induced drag created by the bound vortices located on the planform surfaces, which is of primary importance, can be determined for any given loading and operating condition by utilizing the following basic laws and theorems: Biot-Savart Law, Kutta-Joukowski Theorem, and Munk's Theorems I and II.

Munk's first theorem (Ref. 4) can be stated as follows:

> The total induced drag of any multi-plane lifting system is unaltered if any of the lifting elements are moved in the direction of the motion provided that the attitude of the elements is adjusted to maintain the same distribution of lift among them.

This theorem is commonly referred to as "Munk's stagger theorem." An illustration of this theorem is shown in figure 2-2. Several practical applications can be reasoned from this theorem. First, the chordwise distribution of pressure does not affect the theoretical induced drag of the aircraft if constant section lift is maintained. Second, wing sweep or biplane stagger does not affect the theoretical induced drag as long as the spanwise distribution of lift is constant. A third application is that the load from a system of multi-surfaces, such as the wing and horizonal tail, with the same projection in the Y-Z

plane can be made equivalent to a single surface for the purpose of calculating induced drag.

In the following theoretical development, use will be made of Munk's first theorem to combine the chordwise distribution of vorticity into a single chordwise load and to translate all loads into the 0,Y,Z plane.

Munk's second theorem is illustrated in figure 2-3 and can be stated as follows:

> In calculating the total induced drag of a lifting system, once all the forces have been concentrated into the 0,Y,Z plane, one may, instead of using the actual values of the velocity normal to the lifting elements [$V_n(x,y,z)$] at the original points of application of the forces, use one-half of the limiting value of the normal velocity [$V_n(\infty,y,z)$] for the corresponding values at points P(0,y,z).

This theorem allows the computations to be done in the Trefftz plane, a plane which is located infinitely far downstream, rather than in the real plane. In the subsequent theoretical derivation, this fact will be utilized in order to make all the induced drag computations in the Trefftz plane, thereby greatly simplifying the calculations.

The third theorem given by Munk is presented as follows:

> When all the elements of a lifting system have been translated longitudinally to a single plane, the induced drag will be a minimum when the

> component of the induced velocity normal to the lifting element at each point is proportional to the cosine of the angle of inclination of the lifting element at that point.

This theorem is illustrated in figure 2-4 and can be summarized in equation form as:

$$V_n = w_o \cos \theta \qquad 2.1$$

For a horizonal lifting element it can be seen from equation (2.1) that the normal velocity (downwash) across the span is equal to a constant. For a vertical plane (θ =90 degrees), the normal velocity (sidewash) must be equal to zero for minimum induced drag. The physical interpretation of this theorem will be further illustrated in a subsequent section.

The basic equation for calculating the induced drag can be derived by applying the Kutta-Joukowsaki theorem in the drag direction. By utilizing Munk's theorems, the calculations can be accomplished in the Trefftz plane. Thus, the basic equation for calculating the induced drag for an arbitrary non-planer lifting system, expressed in terms of the Trefftz plane and using vector notation is:

$$D_i = \frac{1}{2V_\infty} \int \bar{V} \cdot \bar{n} \, N \, d\ell \qquad 2.2$$

This integral is a line integral taken around the perimeter of the projection of the lifting surface in the

Trefftz plane. The vector $\bar{V}$ is the resultant induced velocity vector in the Trefftz plane from all horseshoe vortices located on the load perimeter. N represents the load perimeter normal force per unit span. For a horizonal lifting surface, N would represent the section lift force. The vector $\bar{n}$ is a unit vector, normal to the load perimeter.

Physical Interpretation of Theoretical Concepts

To provide a better understanding of induced drag calculations, the theoretical concepts discussed in the previous section will be illustrated using a monoplane wing-winglet configuration. In figure 2-6 the sources of induced drag for a wing-winglet configuration are shown. They are:

Induced drag due to the induced flow by the wings on the wing

Induced drag due to the induced flow by the wings on the winglet

Induced drag due to the induced flow by the winglets on the wing

Induced drag due to the induced flow by the winglets on the winglet

For simplicity, the effects of symmetry are included in the sources of induced drag shown and are not delineated separately.

In figure 2-5a the effect of the wing induced flow is shown. The wing under positive load produces a downwash on itself which results in the wing force vector, $\bar{F}$, tilting rearward by an angle α_i. The wing force vector is perpendicular to the resultant velocity vector, $\bar{V}$, by definition of the Kutta-Joukowski theorem. A sidewash is also produced by the wing at the winglet. As can be seen in figure 2-5b, the sidewash at the winglet combined with the freestream velocity produces a tilt forward of the resultant winglet force vector. This produces a negative drag component as well as a side force component on the winglet.

In figure 2-5c, the induced drag resulting from the sidewash induced by the winglet on itself is presented. This results in a rearward tilting of the resultant force vector, which creates an attendant induced drag component as well as an additional side force component. It should be noted that the direction of the winglet force vector is consistant with a positive (upload) on the wing. The winglet also induces an upwash on the wing. In figure 2-5d it can be seen that this upwash rotates the resultant wing force vector forward. This produces an additional lift force on the wing as well as a negative drag component.

The results of figures 2-5a, 2-5b, 2-5c, and 2-5d are summarized in figure 2-6, where all the induced velocities are combined. For minimum induced drag, equation (2.1) indicates that the velocity normal to the winglet must be

equal to zero. This can be seen to occur when the sidewash produced on the winglet by the wing exactly cancels the sidewash produced by the winglet on itself. In other words, the induced angle of attack of the winglet is zero. The induced drag of the wing is also minimized by the presence of a winglet since the winglet causes a reduction in the net downwash at the wing; hence, the induced angle of attack is reduced. Also, the winglets allow the wing to be loaded more heavily out towards the tips, which of course results in a more efficient wing.

Theoretical Application

The Vortex-Lattice Computer Program

The purpose of this section is to present and discuss the methods used in developing the vortex-lattice computer program. Relevant equations and formulas will be discussed in order that the reader may understand, and if necessary, modify the existing program. Figure 2-7 shows the computer program flowchart which represents the internal structuring of the vortex-lattice computer program.

The first function performed by the program is the input of the biplane-winglet planform geometry, as well as the input of data representing a given flight condition. Upon execution of the program, the computer will prompt the user for the following: biplane aspect ratio, biplane stagger, decalage angle, wing twist, maximum winglet toe

angle, and angle of attack. The wings and winglets are assumed to have no camber or taper, and the biplane gap is held constant at one chord length. Since the flow is inviscid and incompressible, the velocity may be arbitrarily chosen.

The next function performed, after the total number of spanwise and chordwise horseshoe vortices have been determined, is the computation of the coordinates of all the horseshoe vortices and their cooresponding control points. In this program, the number of chordwise and spanwise horseshoe vortices is pre-set. The upper and lower wings each contain a total of 80 horseshoe vortices (40 located spanwise and 2 located chordwise for each wing), while the winglets each contain a total of 16 horseshoe vortices (8 located spanwise and 2 located chordwise for each winglet). These numbers were arrived at by analyzing output data from several program executions, and choosing numbers which would yield converging results without consuming enormous computational time.

In constructing the vortex-lattice planform model, only a half-span model is constructed since a symmetrical loading is assumed. The program computes the position of each horseshoe vortex, represented by pn_n, qn_n, rn_n, where the subscript n represents the n^{th} horseshoe vortex. Similarily, the program also computes the position of each corresponding control point, represented by pv_ν, qv_ν, rv_ν,

where the subscript ν represents the position of the ν^{th} control point. This is accomplished by applying the 1/4-3/4 rule to each elemental panel. Figure 2-8 shows the half-span planform model of the biplane-winglet configuration represented by a system of rectangular horseshoe vortices. In this model, Γ_1 through Γ_{40} are located on the upper wing, Γ_{41} through Γ_{80} are located on the lower wing, and Γ_{81} through Γ_{96} are located on the starboard winglet. The P,Q,R axis system is also shown with the origin located at the mid-span point of the leading edge of the upper wing.

Since a symmetrical loading is assumed, the tangential flow boundary condition will be applied only to the control points located on the starboard planform. However, the total induced velocity at each control is contributed to by each and every bound horseshoe vortex located on both the starboard and port planforms. Because of the symmetrical loading assumption, Γ_n on the starboard wing is equal to Γ_n on the port wing. Therefore, only the half-span horseshoe vortex strength distribution must be solved for.

Next, the coordinates, $P_{\nu n}$, of the ν^{th} control point relative to the n^{th} horseshoe vortex can be computed in the X,Y,Z axis system. For the starboard wing:

$$P_{\nu n} = (x_{\nu n}, ys_{\nu n}, z_{\nu n})$$

$$x_{\nu n} = p\nu_\nu - pn_n$$

$$ys_{\nu n} = q\nu_\nu - qn_n$$

$$z_{\nu n} = r\nu_\nu - rn_n$$

and for the port wing:

$$P_{\nu n} = (x_{\nu n},\ yp_{\nu n},\ z_{\nu n})$$

$$x_{\nu n} = p\nu_{\nu} - pn_{n}$$

$$yp_{\nu n} = q\nu_{\nu} + qn_{n}$$

$$z_{\nu n} = r\nu_{\nu} - rn_{n}$$

The influence coefficients, which relate the induced velocity at the ν^{th} control point to the strength of the n^{th} horseshoe vortex (which is inducing the flow at that control point) must be computed next. They are computed in order to determine the vortex induced velocity at each of the control points located on the starboard planform.

The downwash influence coefficients, which represent the induced velocities caused by the bound horseshoe vortices located on the starboard planform, can be computed from the following expression. The angle ϕ represents the angle of the bound horseshoe vortex filament in the P-R plane. For the horizonal surface (wing), ϕ =0 degrees, and for the vertical surface (winglet), ϕ =90 degrees.

$$Fws_{\nu n} = \frac{-x_{\nu n}\cos\phi_n}{x_{\nu n}^2+(Z_{\nu n}\cos\phi_n - ys_{\nu n}\sin\phi_n)^2}$$

$$\cdot\left\{\frac{(ys_{\nu n}+s\cos\phi_n)\cos\phi_n+(Z_{\nu n}+s\sin\phi_n)\sin\phi_n}{[x_{\nu n}^2+(ys_{\nu n}+s\cos\phi_n)^2+(Z_{\nu n}+s\sin\phi_n)^2]^{\frac{1}{2}}}\right.$$

$$- \frac{(ys_{\nu n} - s \cos \phi_n)\cos \phi_n + (Z_{\nu n} - s \sin \phi_n)\sin \phi_n}{[x_{\nu n}^2 + (ys_{\nu n} - s \cos \phi_n)^2 + (Z_{\nu n} - s \sin \phi_n)^2]^{1/2}}$$

$$- \frac{(ys_{\nu n} - s \cos \phi_n)}{(ys_{\nu n} - s \cos \phi_n)^2 + (Z_{\nu n} - s \sin \phi_n)^2}$$

$$\cdot \left\{ 1 - \frac{x_{\nu n}}{[x_{\nu n}^2 + (ys_{\nu n} - s \cos \phi_n)^2 + (Z_{\nu n} - s \sin \phi_n)^2]^{1/2}} \right\}$$

$$+ \frac{(ys_{\nu n} + s \cos \phi_n)}{(ys_{\nu n} + s \cos \phi_n)^2 + (Z_{\nu n} + s \sin \phi_n)^2}$$

$$\cdot \left\{ 1 - \frac{x_{\nu n}}{[x_{\nu n}^2 + (ys_{\nu n} + s \cos \phi_n)^2 + (Z_{\nu n} + s \sin \phi_n)^2]^{1/2}} \right\}$$

Similarily, the downwash influence coefficients which represent the port wing can be expressed identically to the above equation except $yp_{\nu n}$ is substituted in place of $ys_{\nu n}$. The downwash at the ν^{th} control point, induced by the n^{th} horseshoe vortex located on the port and starboard planform, represented by $w_{\nu n}$, can be expressed as:

$$w_{\nu n} = \frac{\Gamma_n}{4\pi} (Fws_{\nu n} + Fwp_{\nu n}) \qquad 2.3$$

In a similar manner, the sidewash velocity at the ν^{th} control point induced by the n^{th} horseshoe vortex can be computed. The sidewash influence coefficients representing the bound vortices on the starboard wing can be computed from the following expression(Ref. 15).

$$Fvs_{\nu n} = \frac{-x_{\nu n} \sin \phi_n}{x_{\nu n}^2 + (Z_{\nu n} \cos \phi_n - ys_{\nu n} \sin \phi_n)^2}$$

$$\cdot \left\{ \frac{(ys_{\nu n} + s \cos \phi_n)\cos \phi_n + (Z_{\nu n} + s \sin \phi_n)\sin \phi_n}{[x_{\nu n}^2 + (ys_{\nu n} + s \cos \phi_n)^2 + (Z_{\nu n} + s \sin \phi_n)^2]^{\frac{1}{2}}} \right.$$

$$\left. - \frac{(ys_{\nu n} - s \cos \phi_n)\cos \phi_n + (z_{\nu n} - s \sin \phi_n)\sin \phi_n}{[x_{\nu n}^2 + (ys_{\nu n} - s \cos \phi_n)^2 + (Z_{\nu n} - s \sin \phi_n)^2]^{\frac{1}{2}}} \right\}$$

$$+ \frac{(Z_{\nu n} - s \sin \phi_n)}{(ys_{\nu n} - s \cos \phi_n)^2 + (Z_{\nu n} - s \sin \phi_n)^2}$$

$$\cdot \left\{ 1 - \frac{x_{\nu n}}{[x_{\nu n}^2 + (ys_{\nu n} - s \cos \phi_n)^2 + (Z_{\nu n} - s \sin \phi_n)^2]^{\frac{1}{2}}} \right\}$$

$$- \frac{Z_{\nu n} + s \sin \phi_n}{(ys_{\nu n} + s \cos \phi_n)^2 + (Z_{\nu n} + s \sin \phi_n)^2}$$

$$\cdot \left\{ 1 - \frac{x_{\nu n}}{[x_{\nu n}^2 + (ys_{\nu n} + s \cos \phi_n)^2 + (Z_{\nu n} + s \sin \phi_n)^2]^{\frac{1}{2}}} \right\}$$

The sidewash influence coefficients representing the port planform can be expressed as above except $yp_{\nu n}$ is again substituted in place of $ys_{\nu n}$. Similarily, the sidewash velocity at the ν^{th} control point induced by the n^{th} horseshoe vortex located on both the port and starboard planform, represented by $v_{\nu n}$, can be expressed as:

$$v_{\nu n} = \frac{\Gamma_n}{4\pi} (Fvs_{\nu n} + Fvp_{\nu n}) \qquad 2.4$$

The total downwash at a given control point is equal to the sum of the induced downwash contributions from each horseshoe vortex located on the entire planform surface. The total downwash at the ν^{th} control point can be computed from the following:

$$w_\nu = \sum_{n=1}^{N} w_{\nu n} = \sum_{n=1}^{N} \left[\frac{\Gamma_n}{4\pi} \left(Fws_{\nu n} + Fwp_{\nu n}\right)\right] \qquad 2.5$$

Similarily, the total sidewash at a given control point can be expressed as

$$v_\nu = \sum_{n=1}^{N} v_{\nu n} = \sum_{n=1}^{N} \left[\frac{\Gamma_n}{4\pi} \left(Fvs_{\nu n} + Fvp_{\nu n}\right)\right] \qquad 2.6$$

Next, the tangential flow boundary condition at each of the control points located on the starboard planform must be satisfied. First the horizonal (wing) planform surface will be considered. By equating the freestream velocity and

local angle of attack to the local downwash velocity, the following boundary condition for the ν^{th} control point can be formulated.

$$\sum_{\nu=1}^{M} \alpha_\nu = \frac{1}{V_\infty} \sum_{\nu=1}^{M} \sum_{n=1}^{N} w_{\nu n} \qquad 2.7$$

This can also be expressed as:

$$\sum_{\nu=1}^{M} \alpha_\nu = \frac{1}{4\pi V_\infty} \sum_{\nu=1}^{M} \sum_{n=1}^{N} \left[\Gamma_n \left(Fws_{\nu n} + Fwp_{\nu n}\right)\right] \qquad 2.8$$

where α_ν represents the local angle of attack of the control point. M represents the number of horseshoe vortices and cooresponding control points located on the horizonal planform surface, and N represents the number of vortices and control points located on both the horizonal and vertical planform surfaces. Expanding equation (2.8) yields M linear equations; each equation containing N unknown circulation strengths. They can be expanded to the following:

$$\Gamma_1(Fws_{1,1} + Fwp_{1,1}) + \Gamma_2(Fws_{1,2} + Fwp_{1,2}) + \ldots + \Gamma_N(Fws_{1,N} + Fwp_{1,N}) = 4\pi V_\infty \alpha_1$$

$$\Gamma_1(Fws_{2,1} + Fwp_{2,1}) + \Gamma_2(Fws_{2,2} + Fwp_{2,2}) + \ldots + \Gamma_N(Fws_{2,N} + Fwp_{2,N}) = 4\pi V_\infty \alpha_2$$

$$\vdots$$

$$\Gamma_1(Fws_{M,1} + Fwp_{M,1}) + \Gamma_2(Fws_{M,2} + Fwp_{M,2}) + \ldots + \Gamma_N(Fws_{M,N} + Fwp_{M,N}) = 4\pi V_\infty \alpha_M$$

The remaining linear equations can be derived by applying the same tangential flow boundary condition to the vertical surfaces. This boundary condition can be written as:

$$\sum_{\nu=M+1}^{N} i_\nu = \frac{1}{V_\infty} \sum_{\nu=M+1}^{N} \sum_{n=1}^{N} v_{\nu n} \qquad 2.9$$

where i_ν represents the incident angle of attack (toe angle) of the winglet. This can also be written as:

$$\sum_{\nu=M+1}^{N} i_\nu = \frac{1}{4\pi V_\infty} \sum_{\nu=M+1}^{N} \sum_{n=1}^{N} \left[\Gamma_n \left(Fvs_{\nu n} + Fvp_{\nu n}\right)\right] \qquad 2.10$$

Expanding this yields the remaining linear equations necessary to determine the unknown circulation strengths.

$$\Gamma_1(Fvs_{M+1,1} + Fvp_{M+1,1}) + \Gamma_2(Fvs_{M+1,2} + Fvp_{M+1,2}) + \ldots + \Gamma_N(Fvs_{M+1,N} + Fvp_{M+1,N}) = 4\pi V_\infty i_{M+1}$$

$$\Gamma_1(Fvs_{M+2,1} + Fvp_{M+2,1}) + \Gamma_2(Fvs_{M+2,2} + Fvp_{M+2,2}) + \ldots + \Gamma_N(Fvs_{M+2,N} + Fvp_{M+2,N}) = 4\pi V_\infty i_{M+2}$$

$$\vdots$$

$$\Gamma_1(Fvs_{N,1} + Fvp_{N,1}) + \Gamma_2(Fvs_{N,2} + Fvp_{N,2}) + \ldots + \Gamma_N(Fvs_{N,N} + Fvp_{N,N}) = 4\pi V_\infty i_N$$

Finally, the unknown circulation strengths can be computed by simultaniously solving the complete set of linear algebraic equations. This can easily be done by first expressing the equations in matrix form as:

$$[A]\{\Gamma_n\} = \{B\}$$

where [A] is the coefficient matrix, and {B} is the boundary condition matrix. The solution can be obtained by inverting the coefficient matrix and multiplying it by the boundary condition matrix.

$$\{\Gamma_n\} = [A]^{-1}\{B\}$$

The wing and winglet section loading coefficients can now be computed from the known circulation strengths using the following well-known relationship.

$$C_\ell = \frac{2\Gamma}{c\ V_\infty} \qquad 2.11$$

The total lift produced by the upper and lower wings can be expressed as:

$$L = 2\int_0^{b/2} \rho\ V_\infty\ \Gamma(y)\ dy \qquad 2.12$$

Expressing this in lift coefficient form yields:

$$C_{L_w} = \frac{4}{V_\infty S_w}\int_0^{b/2} \Gamma(y)\ dy \qquad 2.13$$

Converting this into a numerical integration form results in:

$$C_{L_w} = \frac{4}{V_\infty S_w}\sum_{n=1}^{M} \Gamma_n\ 2s \qquad 2.14$$

Similarily, the side force coefficient for the winglet can be expressed as:

$$C_{L_{w\ell}} = \frac{2}{V_\infty S_{w\ell}} \sum_{n=M+1}^{N} \Gamma_n \, 2s \qquad 2.15$$

The induced drag coefficients are computed next by first calculating the total vortex induced velocities, normal to the control points on the load perimeter in the Trefftz plane. This is done by first calculating the position coordinates of the ν^{th} control point (in the Trefftz plane) relative to the n^{th} horseshoe vortex as follows:

$$x_{\nu n} = -\infty$$

$$ys_{\nu n} = q\nu_\nu - qn_n$$

$$yp_{\nu n} = q\nu_\nu + qn_n$$

$$z_{\nu n} = r\nu_\nu - rn_n$$

The influence coefficients are then recalculated. By knowing the circulation strengths of each horseshoe vortex, the downwash velocity normal to each control point on the horizonal planform in the Trefftz plane can be computed as well as computing the sidewash velocity normal to each control point on the vertical planform surface. Thus, by virtue of Munk's theorems and the Kutta-Joukowsi theorem, the induced drag coefficients can be computed.

The induced drag coefficient, $C_{D_{w,w}}$, which is caused by the wing inducing a downwash on itself, can be computed from the following expression:

$$C_{D_{w,w}} = \frac{4}{V_\infty^2 S_w} \sum_{n=\nu=1}^{M} w_{\nu_w} \Gamma_n s \qquad 2.16$$

where w_{ν_w} represents the downwash induced at the ν^{th} control point by the wing. The induced drag coefficient, $C_{D_{wl,w}}$, which is caused by the winglet inducing an upwash on the wing, can be computed from the following:

$$C_{D_{wl,w}} = \frac{4}{V_\infty^2 S_w} \sum_{n=\nu=1}^{M} w_{\nu_{wl}} \Gamma_n s \qquad 2.17$$

where $w_{\nu_{wl}}$ represents the upwash induced at the ν^{th} control point by the winglet.

Similarily, the induced drag coefficients, $C_{D_{w,wl}}$ and $C_{D_{wl,wl}}$, which are caused by the wing and winglet inducing a sidewash on the winglet, can be expressed as follows:

$$C_{D_{wl,wl}} = \frac{4}{V_\infty^2 S_w} \sum_{n=\nu=M+1}^{N} v_{\nu w_l} \Gamma_n s \qquad 2.18$$

$$C_{D_{w,wl}} = \frac{4}{V_\infty^2 S_w} \sum_{n=\nu=M+1}^{N} u_{\nu_w} \Gamma_n s \qquad 2.19$$

The total induced drag is then equal to the sum of the four induced drag coefficients. It is of interest to note that the wing induces a negative drag component on the winglet,

and similarily, the winglet induces a negative drag component on the wing. The wing efficiency factor can be calculated from the following expression:

$$e = \frac{\partial C_L}{\partial C_{D_i}} \frac{1}{\pi AR} \qquad 2.20$$

The theoretical drag polar can be now be computed. However, first the minimum profile drag and the incremental change in profile drag due to lift must be added to the induced drag term to yield the total drag coefficient.

$$C_D = C_{D_{min}} + \Delta C_{D_p} + C_{D_i} \qquad 2.21$$

Finally, the three-dimensional lift-curve slope can be determined once the lift coefficient has been determined for different angles of attack.

As was expressed previously, it is common in biplane theory to compute the wing efficiency factor utilizing the biplane's equivalent monoplane aspect ratio. The equivalent monoplane aspect ratio can be calculated from the following expression:

$$EMAR = \frac{b_1^2}{S} \frac{\mu^2(1+\gamma)^2}{(\mu^2 + 2\sigma\mu\gamma + \gamma^2)}$$

b_1 upper wing span

μ $\frac{\text{lower wing area}}{\text{upper wing area}}$

σ from Figure 186 (Ref. 20)

γ $\frac{\text{lower wing span}}{\text{upper wing span}}$

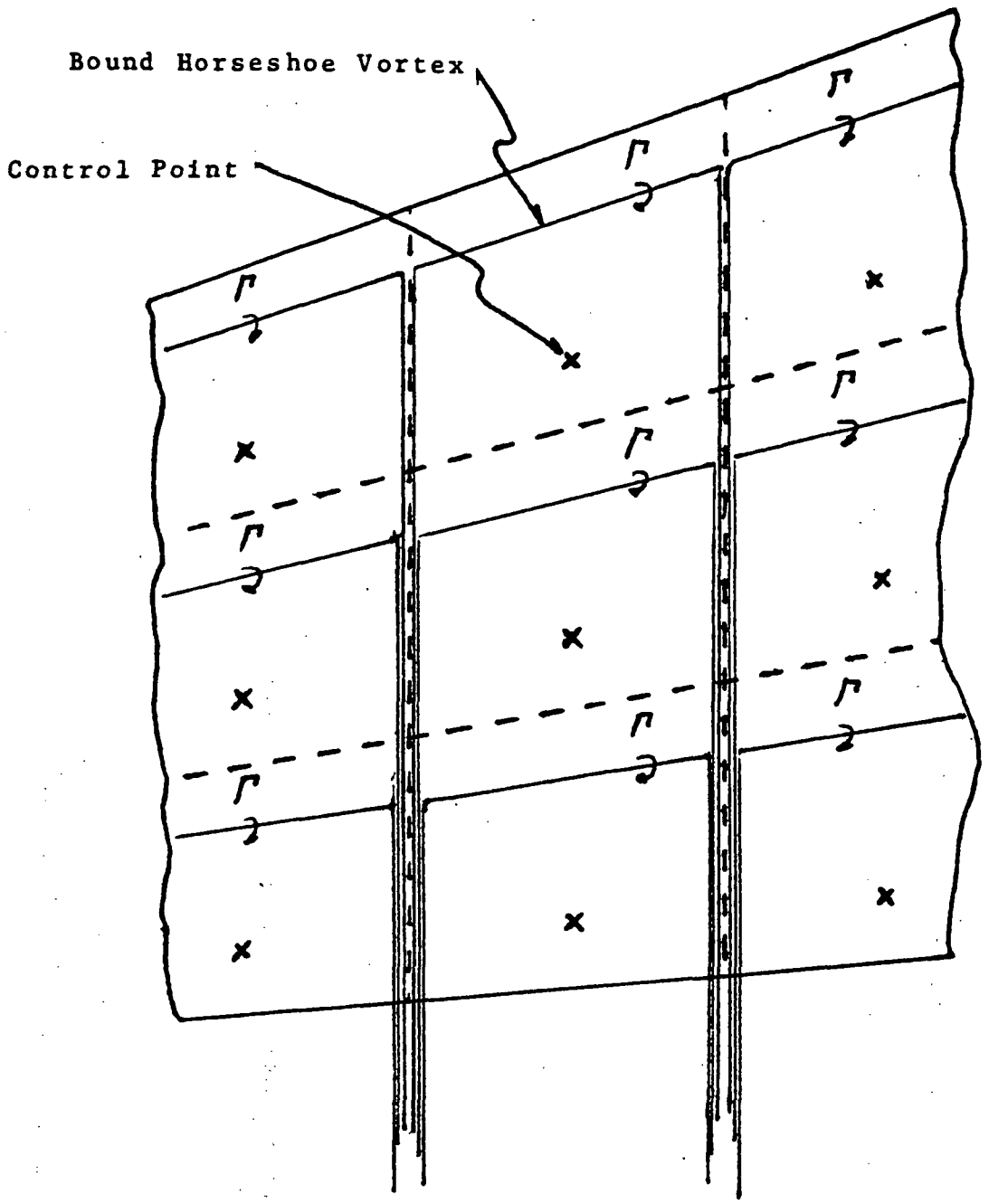

Figure 2-1 Typical Vortex-Lattice Representation

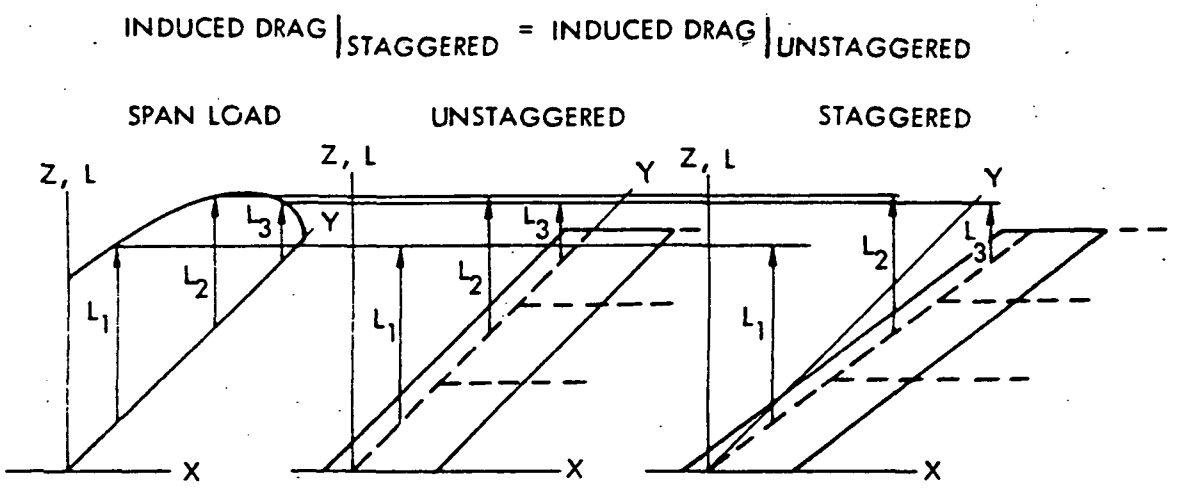

Figure 2-2 Illustration of Munk's First Theorem

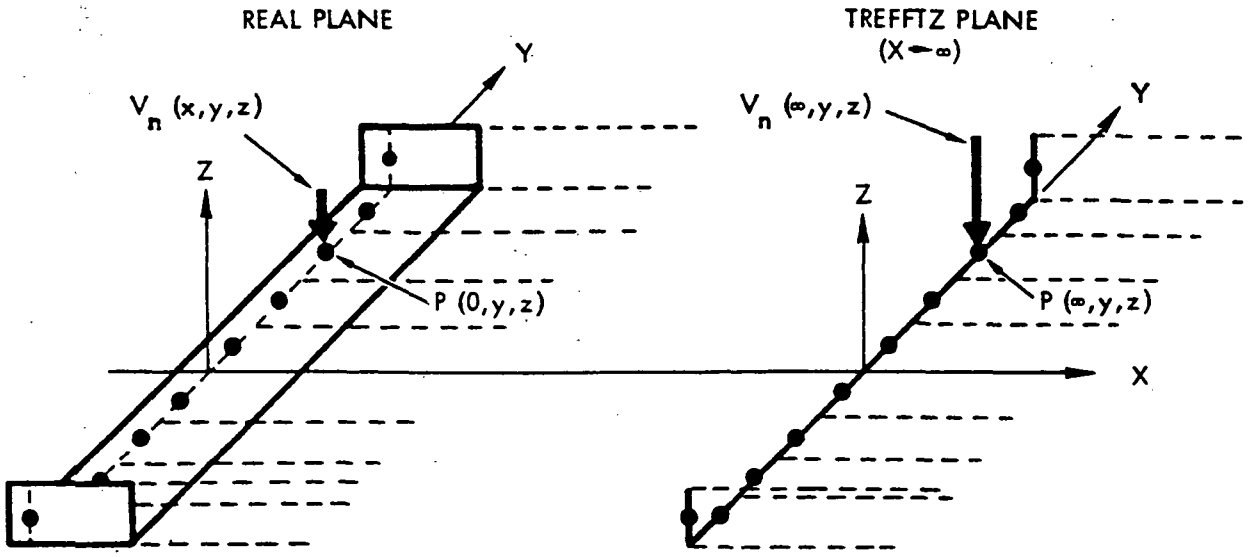

Figure 2-3 Illustration of Munk's Second Theorem

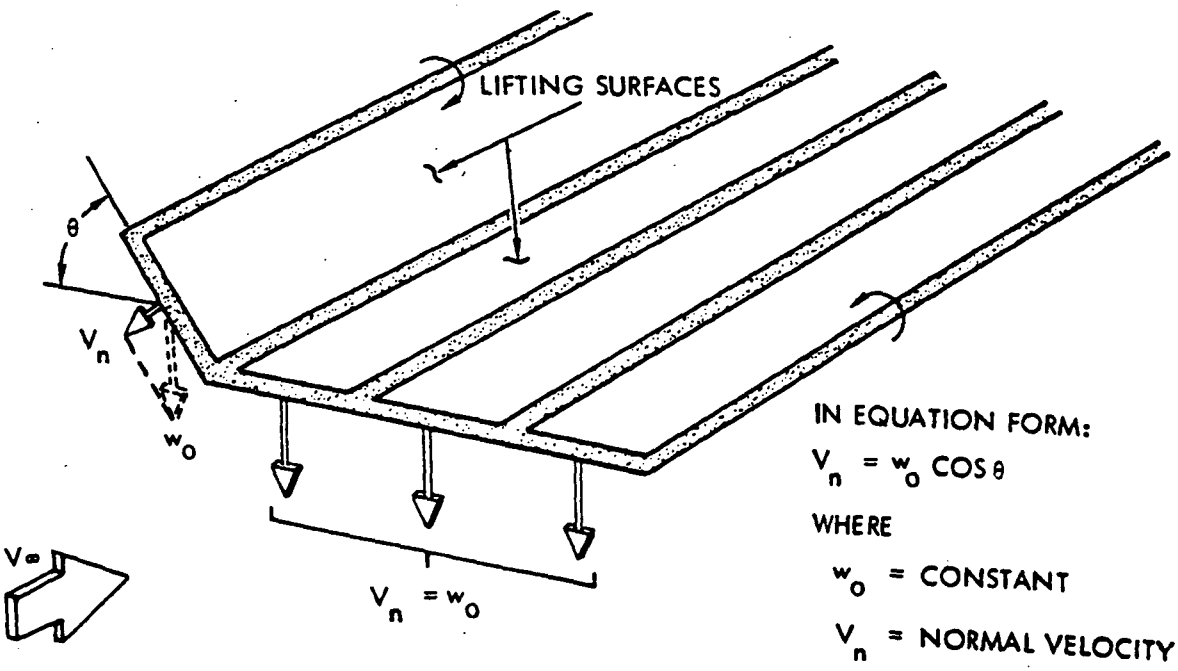

Figure 2-4 Illustration of Munk's Third Theorem

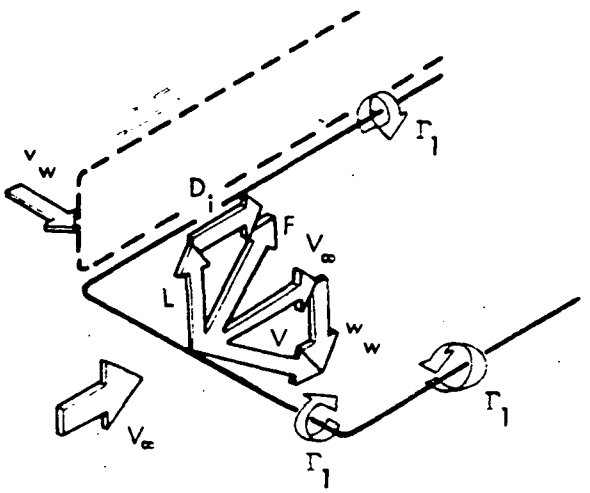

(a) Drag due to wing on wing $D_{i_{w,w}}$.

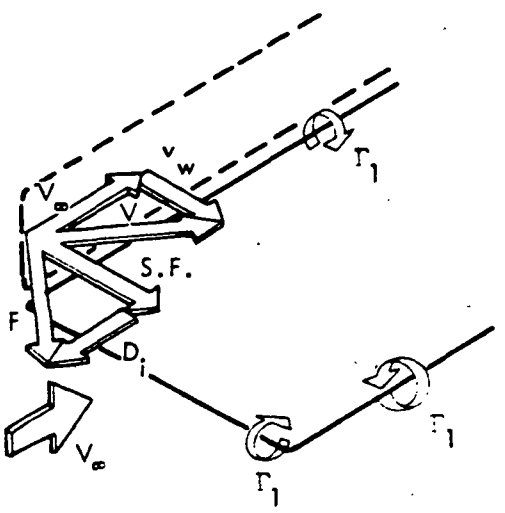

(b) Drag due to wing on winglet $D_{i_{w,wl}}$.

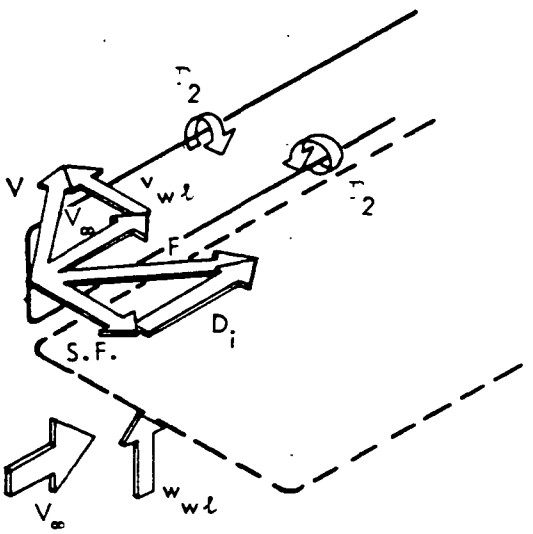

(c) Drag due to winglet on winglet $D_{i_{wl,wl}}$.

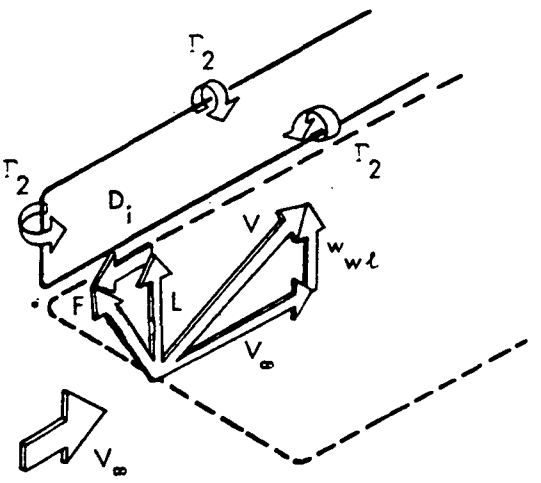

(d) Drag due to winglet on wing $D_{i_{wl,w}}$.

Figure 2-5 Sources of Induced Drag for a Wing-Winglet Configuration

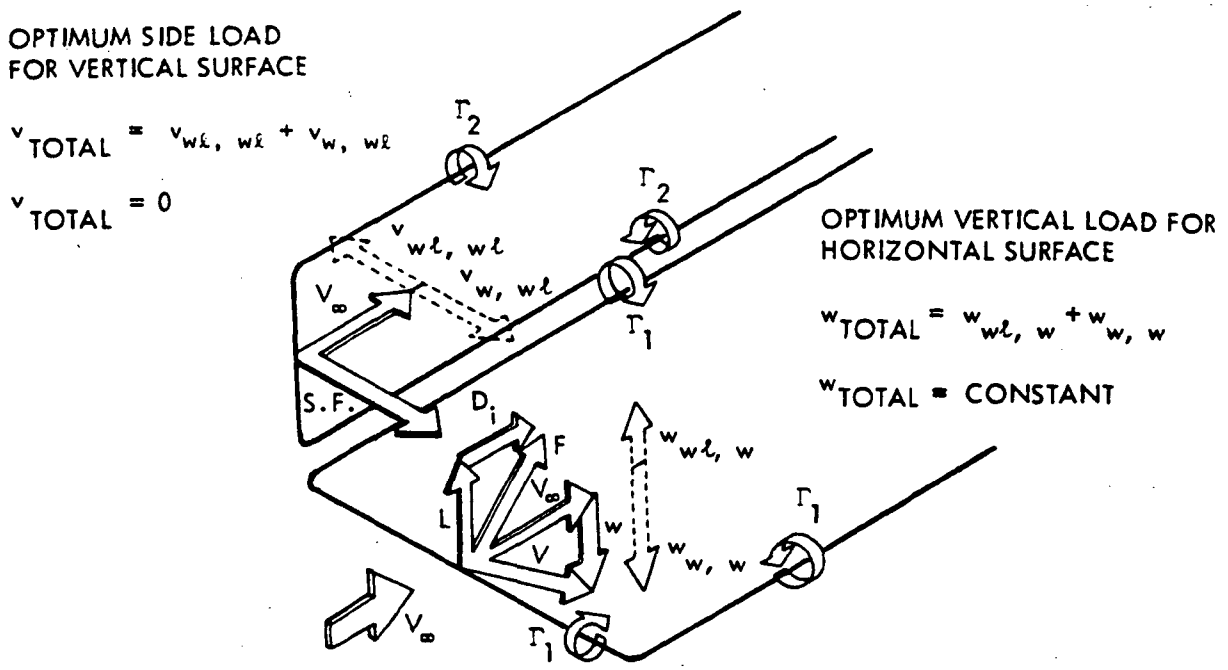

Figure 2-6 Combined Sources of Induced Drag for a Wing-Winglet Configuration

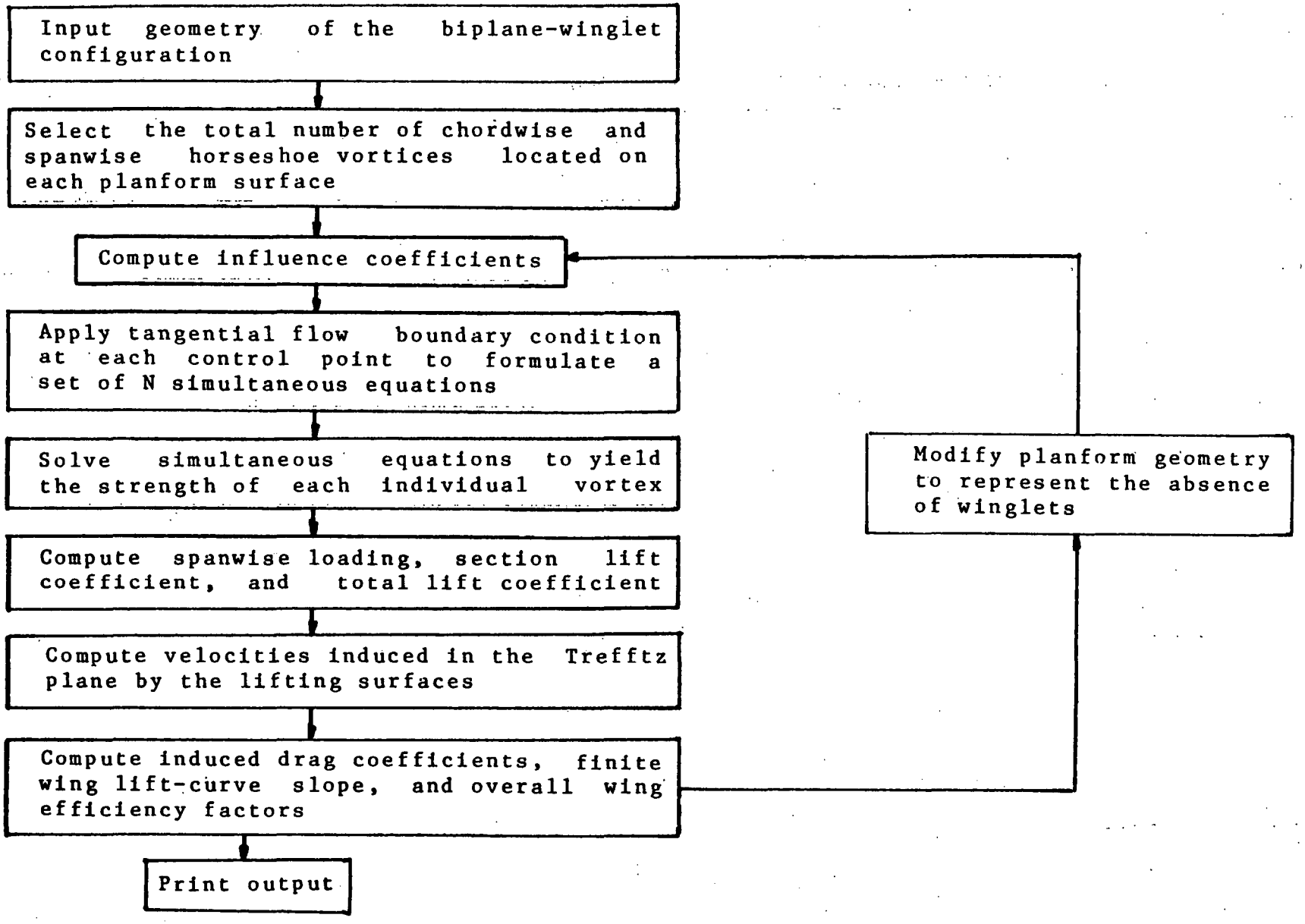

Figure 2-7 Vortex-Lattice Computer Program Flowchart

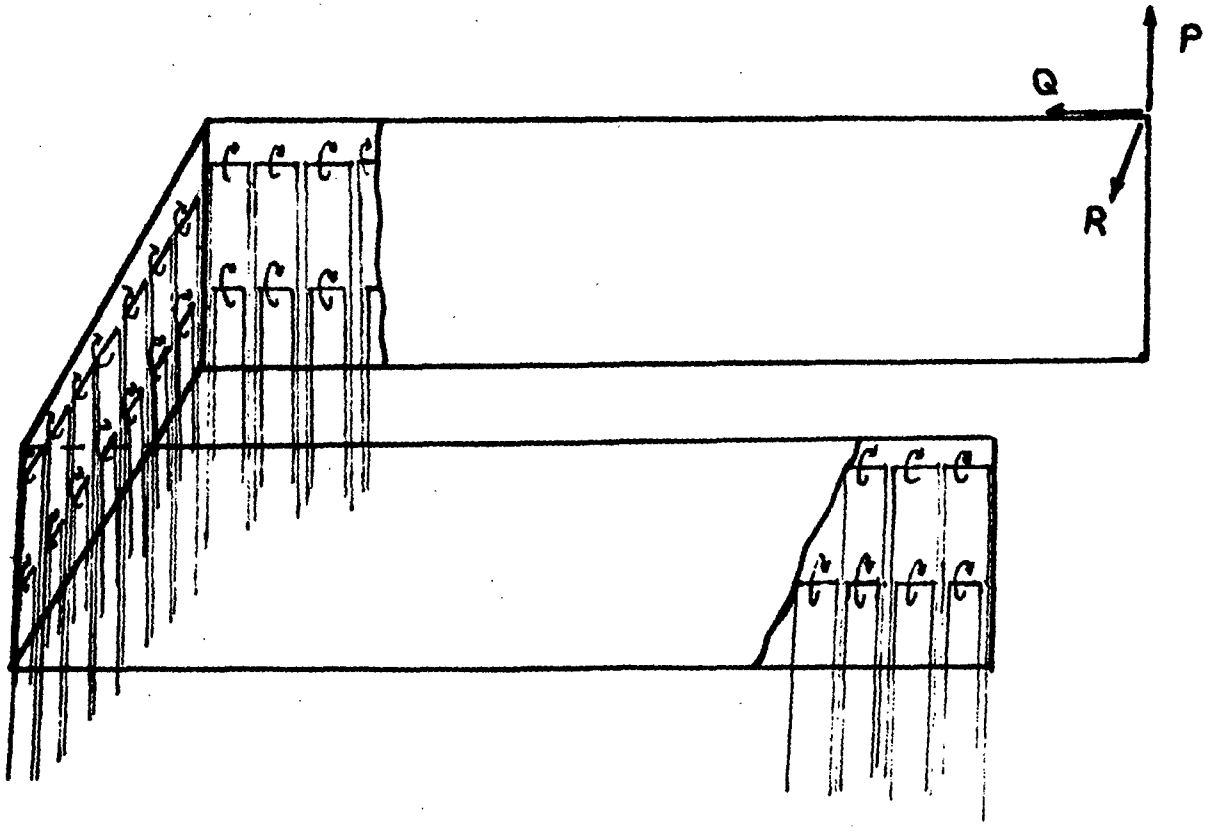

Figure 2-8 Biplane-Winglet Vortex-Lattice Representation

CHAPTER III

EXPERIMENTAL APPARATUS AND PROCEDURE

Before conclusions can be drawn on the aerodynamic characteristics and performance of the biplane-winglet configuration as predicted by the vortex-lattice computer program, experimental data must be collected, correlated, and analyzed to determine the validity of the theoretical predictions.

Description of Apparatus

For the purpose of obtaining experimental data, a half-span wind-tunnel model of the biplane-winglet configuration was constructed by the author and tested in The Pennsylvania State University's atmospheric closed-return subsonic wind tunnel. A half-span model was tested, which was mounted vertically in the wind tunnel, extending upward through the floor of the test section. The model was designed and constructed to have a stagger of one chord length, a gap of one chord length, and a decalage angle that could be varied from 0 to -6 degrees. The design of the model's geometric configuration was based on the already optimized design configurations found by Nenadovitch and Olson in previous wind tunnel experimentation utilizing biplane configurations.

The two finite wings utilized in the model were constructed from solid mohogany using a router-assembly tool designed specifically for this purpose. The airfoil used was a NACA 0012, and the wing's cross-section profile was sanded to within 0.015 inches of the exact NACA 0012 airfoil specifications. The two wings, which are identical, have a chord length of 7.875 inches, a half-span of 19.75 inches, and a maximum cross-sectional thickness of 0.96 inches. This yields an aspect ratio of five, since the configuration tested represents a half-span model.

Spanning the tips of the two wings is a constant-chord winglet. The winglet was constructed from pine and was sanded to form a thin 3% thick symmetrical airfoil. The winglet was held in place by four screws, and could easily be removed for conducting tests with and without the winglet attached. Also, by shimming, the winglet toe angle could be varied by as much as plus or minus 2 degrees, although zero incidence was used in the experimental tests. Zero incidence was chosen because the vortex-lattice computer program predicted that no aerodynamic advantages could be gained by having any winglet incidence present. The presence of a high-degree of toe angle incidence caused a slight increase in the induced drag. This was due to the increase in the spanwise load distribution along the winglet. The theoretical cases that were examined assumed the toe angle to be maximum negative where the winglet

joined the upper wing, and maximum positive where the winglet joined the lower wing. The winglet was also assumed to have a linear twist between the points of maximum incidence.

The chord length of the winglet was a constant 7.875 inches, and no cant angle was present. Figure 3-1 shows the model mounted in the four by five foot test section of the subsonic wind tunnel.

The bases of the wings were mounted, using 1/4 inch bolts and angle brackets, to a 20 inch diameter disk plate, which was fabricated from 3/4 inch laminated plywood. To vary the angle of attack of the model, the base disk was rotated about its geometric center. The aft wing was mounted on a 10 inch diameter disk plate which could be rotated about the aft wing's quarter chord point. This allowed the decalage angle to be varied from 0 to -6 degrees. The winglet was designed to be used for decalage angles ranging from 0 to -6 degrees. To reduce interference drag, the wing-winglet joint was filleted with putty during experimental tests. Figure 3-2 shows the biplane-winglet model before being mounted in the wind tunnel.

Located just below the wind tunnel test section is a six channel pyramid type strain guage balance which is used for recording lift and drag forces during wind tunnel testing. The 20 inch diameter base disk, which supports the

model, was mounted on the pyramid balance prior to calibration of the balance for wind tunnel testing.

Experimental Procedure

Before the actual wind tunnel testing could begin, the wind tunnel balance had to be carefully calibrated. This was done by applying known forces on the balance in the lift and side force directions. The side force channel actually indicates the lift force on the biplane configuration. This is due to the non-standard method used in mounting the model vertically upright in the test section instead of horizonally across. Frictionless pulleys, nylon string, a level, and known weights were used to apply exact known loads to the wind tunnel balance. Several calibration tests were conducted and the following errors in the lift and drag measurments were determined; approximately 5-6% errror in the drag force measurments, and approximately 1-2% error in the lift (side) force measurments. The exact amount of error depends on the magnitude and range of the applied forces. The wind tunnel calibration correction factors were later applied in reducing experimental data.

The biplane-winglet configuration was tested in the wind tunnel at a velocity of approximately 149 feet per second. The ambient air temperture in the test section varied from 115 to 120 degrees Farenheit while the barometric pressure was constant at 29.01 inches of mercury.

This resulted in a Reynolds number of approximately 510,000.

In the first set of experimental tests, the biplane configuration was tested with and without winglets at a decalage angle of 0 degrees, and a stagger and gap both equal to one chord length. The angle of attack was varied from -2 to 21 degrees in 2 degree increments. The angle of attack of the biplane configuration is actually the angle of attack of the upper wing, and the decalage angle is the incident angle of attack of the lower wing relative to the upper wing.

In the second set of experimental tests, the same biplane configuration was tested using the same procedure except the decalage angle was changed to -5 degrees. The angle of attack was varied from -4 to 14 degrees, also in 2 degree increments.

Reduction of Experimental Data

The first step in reducing the experimental data was to apply the wind tunnel balance correction factors (previously determined from calibration tests) to the measured lift and drag forces in order to yield the actual lift and drag forces. Next, standard wind tunnel correction factors were applied to yield experimental results that would be equivalent to the results obtained if the model were tested in free air.

The first correction, known as 'horizonal buoyancy', was found to be negligible for the configuration tested. Buoyancy, which results from a thickening boundary layer on the test section walls, causes a decreasing static pressure gradient in the test section.

The next correction, known as 'solid blocking', is caused by the physical constraint of the flow field normal to the flow direction. This results in a local dynamnic pressure increase over the model which tends increase the measured lift and drag forces. Also, due to physical constraints, the flow field surrounding the model's wake is also constrained. This effect, which is known as 'wake blocking', results in an increase in the measured drag force. Solid blocking and wake blocking have the same effect as horizonal buoyancy, which is an increase in the dynamic pressure over the model.

Finally, a correction must be made to the angle of attack. This is also due to the physical constraint of the test section walls, which alter the trailing vortex system behind the wing. This causes a reduction in the effective angle of attack, which is caused by a reduction in the induced downwash.

Tables 3.1 and 3.2 represent the data collected during wind tunnel testing after the wind tunnel correction factors have been applied to the experimental lift and drag data.

The wind-tunnel correction for angle of attack (induced downwash constraint) was found to be negligible.

Table 3.1

Reduced Experimental Data

Stagger= 1.0, Gap= 1.0, Decalage= 0.0

	With winglet		No winglet	
α	C_L	C_D	C_L	C_D
-2	-0.093	0.018	-0.096	0.016
0	0.000	0.017	0.008	0.015
2	0.073	0.018	0.061	0.016
4	0.220	0.024	0.201	0.021
6	0.354	0.036	0.330	0.033
8	0.519	0.061	0.487	0.057
10	0.654	0.089	0.628	0.086
12.5	0.775	0.115	0.726	0.114
14.5	0.791	0.156	0.758	0.148
16.5	0.827	0.230	0.784	0.228
18.5	0.850	0.267	0.819	0.265
21	0.772	0.356	0.753	0.368

Table 3.2

Reduced Experimental Data

Stagger= 1.0, Gap= 1.0, Decalage= -5

	With winglet		No winglet	
α	C_L	C_D	C_L	C_D
-4	-0.081	0.023	-0.091	0.021
-2	0.037	0.022	0.021	0.020
0	0.186	0.027	0.220	0.024
2	0.334	0.038	0.301	0.035
4	0.468	0.057	0.425	0.053
6	0.577	0.075	0.539	0.072
8	0.698	0.104	0.653	0.100
10	0.791	0.131	0.744	0.128
12	0.867	0.163	0.833	0.165
14	0.775	0.260	0.752	0.256

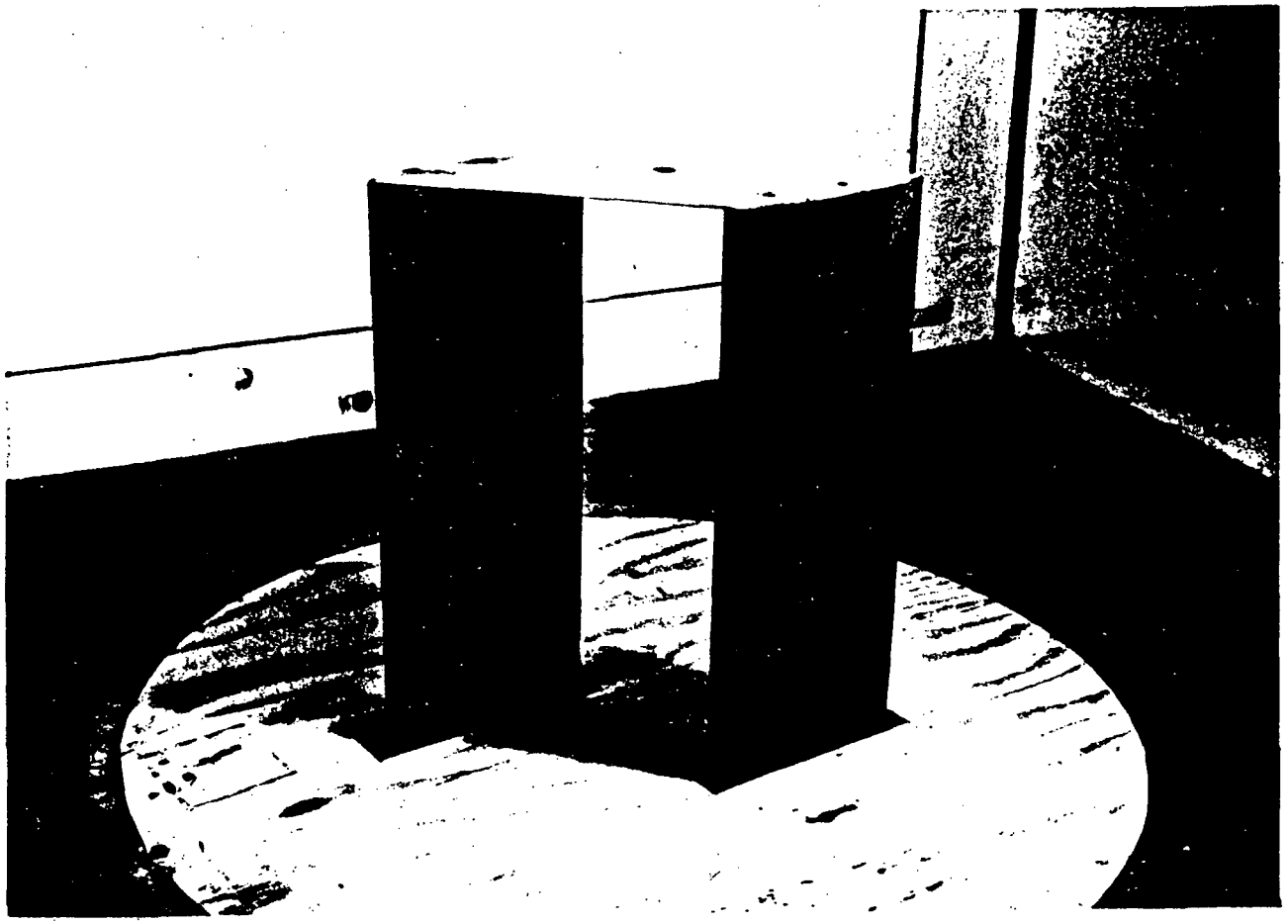

Figure 3-1 Biplane-Winglet Model Mounted in Wind-Tunnel Test Section

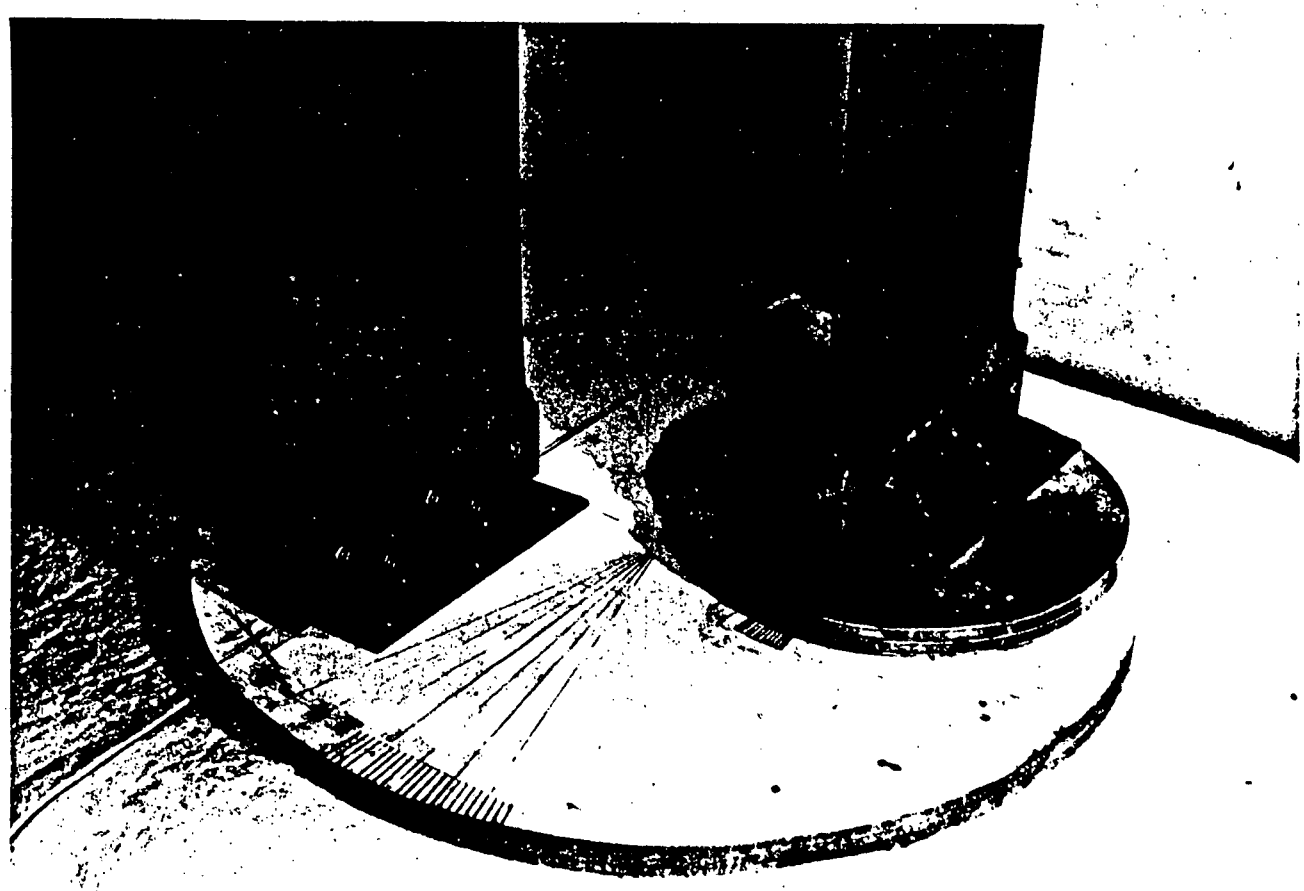

Figure 3-2 Biplane-Winglet Model and Base Support

CHAPTER IV

ANALYSIS OF RESULTS AND DISCUSSION

Overall, the experimental results agreed fairly well with the theoretical vortex-lattice computer program, however, the experimentally determined drag coefficients were found to be quite large. This was discovered to be an effect caused by testing the biplane-winglet configuration in a wind tunnel at a fairly low Reynolds number 510,000.

The following figures and plots, which represent both the theoretical and experimental results, are each shown with two sets of curves; one set represents the results with the winglets attached, while the other represents the results with no winglets. All configurations were tested at a gap and stagger both equal to one chord length.

Figure 4-1 is a plot of the biplane lift coefficient versus angle of attack at a decalage angle of 0 degrees. The experimental results agree quite well with the theoretical results up to an angle of attack of approximately 13 degrees. At this point the upper wing of the biplane begins to stall, while the lower wing remains unstalled until an angle of attack of approximately 18 degrees is reached. Past 18 degrees, both wings are stalled and the lift coefficient drops off rapidly with increasing angle of attack. One of the primary reasons that biplanes

characteristically have a low maximum lift coefficient is because of the asymmetrical stall between the two wings. At a decalage angle of 0 degrees and a stagger of one chord length, the upper wing will operate at a higher lift coefficient than the lower wing. Theory predicts that at an angle of attack of approximately 12 degrees, the upper wing is operating at a C_L of 0.924, while the lower wing is at a C_L of only 0.556. This occurs because the lower wing is emersed in the induced downwash of the upper wing, and hence, the lower wing operates at a less effective angle of attack. This effect does, however, bring on a smooth gradual stall rather than an abrupt stall.

At the test Reynolds number of 510,000, the maximum lift coefficient for the no-winglet configuration was experimentally found to be 0.850. The same configuration tested with winglets showed a 3.6% increase in the maximum lift coefficient. It is expected that a much higher maximum lift coefficient would be reached in full scale flight tests. For example, an NACA 0012 two-dimensional symmetrical airfoil tested at a Reynolds number of 510,000 has a maximum lift coefficient of aproximately 0.900 (Ref. 19) where as the same airfoil tested at a Reynolds number of 6,000,000 yields a maximum lift coefficient of 1.600.

The biplane configuration tested with winglets did show a slight increase in the lift-curve slope as would be expected. The theoretical lift-curve slope without winglets was computed to be 0.059 per degree, while the same configuration with winglets yielded a lift-curve slope of 0.062 per degree; an increase of 5.1%. Experimentally, the lift-curve slope with winglets was 0.064 per degree, while the lift-curve slope without winglets was 0.061 per degree. These values were determined using algebraic linear regression. Also, as would be expected, the theoretical curves continue as a straight line since no flow separation is realized in potential flow theory.

Figure 4-2 is a plot of the biplane lift coefficient versus angle of attack at a decalage angle of -5 degrees. At approximately 12 degrees angle of attack the experimental curve begins to diverge from the theoretical curve due to viscous flow separation. However, in this case the stall occurs much more abruptly due to both wings stalling at approximately the same time. Theory predicts that at an angle of attack of 12 degrees the upper wing is operating at a lift coefficient of 0.912 while the lower wing is at a lift coefficient of 0.953. Therefore, at this decalage angle a nearly symmetrical stall will occur between the two wings. For the no-winglet configuration, $C_{L_{max}}$ was experimentally found to be 0.867 (which is slightly higher than $C_{L_{max}}$ for the no-winglet, zero decalage case). The

biplane configuration (with a decalage angle of -5 degrees) tested with winglets showed a 4.1% increase in the maximum lift coefficient over the no-winglet case.

The theoretical lift-curve slopes for the -5 degree decalage case, with and without winglets, were computed to be 0.057 and 0.054 per degree respectively; a difference of 5.3%. Experimentally, the lift-curve slopes were found to be 0.066 and 0.063 respectively.

It can be reasoned that the change in decalage angle from 0 to -5 degrees has only a slight effect on the lift-curve slopes and the maximum lift coefficient. From figures 4-1 and 4-2 it is obvious that the effect of winglets is a slight increase in the maximum lift coefficient, as well as a slight increase in the lift-curve slopes.

It is well known from previous wind tunnel testing that at low Reynolds numbers, profile drag coefficients can vary quite considerably with only relatively small variations in Reynolds numbers. Therefore, before the experimental data can be properly analyzed, it is desirable to know exactly what effects the low Reynolds numbers will have on profile drag coefficients. The profile drag coefficient, which consists of pressure (form) drag, skin friction drag, interference drag, and parasite drag, is commonly expressed as:

$$C_{D_p} = C_{D_{min}} + \Delta C_{D_p} \qquad 4.1$$

where ΔC_{D_p} is the incremental change in profile drag due to lift. For the biplane-winglet configuration tested in this research, it was necessary to determine the relationship between the incremental profile drag coefficient and the lift coefficient at the test condition Reynolds number of 510,000. This was done by studying the experimental results of Nenadovitch (Ref. 16), who in 1936 performed several experiments to determine the aerodynamic characteristics of two-dimensional biplane configurations utilizing symmetrical airfoils. Figure 4-3 represents a plot of the incremental change in profile drag due to lift for a biplane configuration tested at a Reynolds number of 500,000. For this configuraion, the gap and stagger were both equal to one chord length.

Figures 4-4 and 4-5 represent the experimental and theoretical drag polars for the biplane-winglet configuration tested at 0 and -5 degree decalage angles. The experimental points represent the data taken during wind-tunnel testing after the various wind-tunnel correction factors have been applied. The theoretical curve was plotted utilizing the following equation:

$$C_D = C_{D_{min}} + \Delta C_{D_p} + C_{D_i} \qquad 4.2$$

where $C_{D_{min}}$ is the minimum profile drag coefficient, which for a symmetrical airfoil is also the profile drag

coefficient at zero lift. The values of the minimum profile drag coefficients were determined from wind-tunnel tests. At a decalage angle of 0 degrees, the biplane configuration tested with winglets had a minimum profile drag coefficient of 0.017, while the same configuration without winglets yielded a minimum drag coefficient of 0.015. For the -5 degree decalage case, the test results yielded minimum drag coefficients of 0.022 and 0.020, with and without winglets respectively. Thus, the presence of winglets adds an additional 0.002 to the minimum profile drag coefficient at zero lift. The ΔC_{D_p} term in equation (4.2) was determined using figure 4-3, and the induced drag term, C_{D_i}, was predicted theoretically using the vortex-lattice computer program.

By referring to the drag polars in figures 4-4 and 4-5, the relative advantages of the winglets can be realized. At zero lift, the configuration with winglets produces slightly more drag (parasite drag caused by the presence of the winglets). However, as the lift coefficient begins to increase, the reduction in induced drag caused by the presence of the winglets begins to take affect. At lift coefficients greater than approximately 0.4, the configuration with winglets produces less total drag. This reduction in total drag becomes more significant as the lift coefficient increases further. For the -5 degree decalage case, the total drag is reduced by 6.5% at a lift

coefficient of 0.7, while at a lift coefficient of 0.5 the drag is reduced by 3.3%. For the 0 decalage case, the advantages of adding winglets are not as significant as the -5 degree decalage case, however, above a lift coefficient of 0.4 there is still a reduction in the overall drag caused by the winglets.

The experimental points plotted on the drag polars agree quite well with the theoretical curves, although the experimental points do show a consistantly higher drag contribution. More importantly, the experimental points indicate approximately the same magnitude of drag reduction as do the theoretical curves for both configurations tested.

It is important to realize that if these configurations were tested at a much higher Reynolds number, the induced drag reductions caused by the winglets would be greater. This is due to the significant effect of ΔC_{D_p} at low Reynolds numbers. For example, at an angle of attack of 8 degrees, the biplane configuration with winglets produces a lift coefficient Of 0.519, which is a 6.6% increase over the lift coefficient produced by the same configuration with no winglets. This increase in lift coefficient causes the incremental profile drag coefficient to increase from 0.0144 to 0.0166; an increase of 15.3%. At a Reynolds number of 6,000,000 the profile drag coefficient will increase from 0.0069 to 0.0072; an increase of only 4.3%. Therefore, full-scale advantages of winglets cannot be fully realized

at low Reynolds numbers.

The biplane-winglet efficiency factors were computed by first determining the various slopes of the C_L^2 versus C_D curves. The efficiency factors were calculated based on the actual biplane aspect ratio, which is five. It is common in biplane theory to calculate the efficiency factors based on the biplane's equivalent monoplane aspect ratio, which for this configuration is 3.38. Using the equivalent monoplane aspect ratio would result in a 47% increase in the computed efficiency factors.

Figures 4-6 and 4-7 represent the theoretical and experimental plots of C_L^2 versus C_D for the two decalage cases. The theoretical values were calculated by adding the minimum profile drag coefficient for a specific configuration to the theoretically predicted induced drag coefficients. The experimental points were determined by subtracting the incremental profile drag coefficients from the experimentally determined drag coefficients. The experimental drag coefficients then represent the minimum profile drag plus the induced drag. This was done in order to make logical comparisons between the theoretically predicted and experimentally determined biplane eficiency factors for the various configurations.

For the 0 decalage case, the theoretically predicted efficiency factors were found to be 0.737 and 0.683, with and without winglets respectively. Thus, the addition of winglets causes a theoretical increase in the efficiency factors of 7.9%. The efficiency factors were experimentally determined using algebraic linear regression techniques. The experimental values were determined to be 0.670 and 0.588, with and without winglets respectively, for the 0 decalage case. Thus, a 13.9% increase in efficiency was obtained experimentally by the addition of winglets. Also, it can be noted that the theoretical predictions are approximately 12% higher than the experimental values.

For the -5 degree decalage case, the theoretical efficiency factors were found to to be 0.731 and 0.687, with and without winglets respectively. This is an increase of 6.4%. Experimentally, the efficiency factors with and without winglets were calculated to be 0.663 and 0.562, a difference of 12.6%. Therefore, based on experimental results, the addition of winglets increases the efficiency factors by approximately 13%, which is a significant increase. The 0 degree decalage configuration was experimentally found to yield efficiency factors approximately 5% greater than the -5 degree decalage case, independent of whether winglets were attached or not.

Plots of the theoretically predicted induced drag coefficient as a function of the lift coefficient for the two decalage cases are shown in figures 4-8 and 4-9. It can be observed that as the lift coefficient increases, the reduction in induced drag afforded by the winglets becomes quite significant. At a lift coefficient of 0.6, the addition of winglets theoretically reduces the induced drag by 6.4%, while at a lift coefficient of 0.8, the induced drag is reduced by 8.3%. At a cruise lift coefficient of 0.4 the induced drag is reduced by 6.2%. It is also significant to note that there appears to be little variation in the magnitude of induced drag reduction between the 0 and -5 degree decalage configuration.

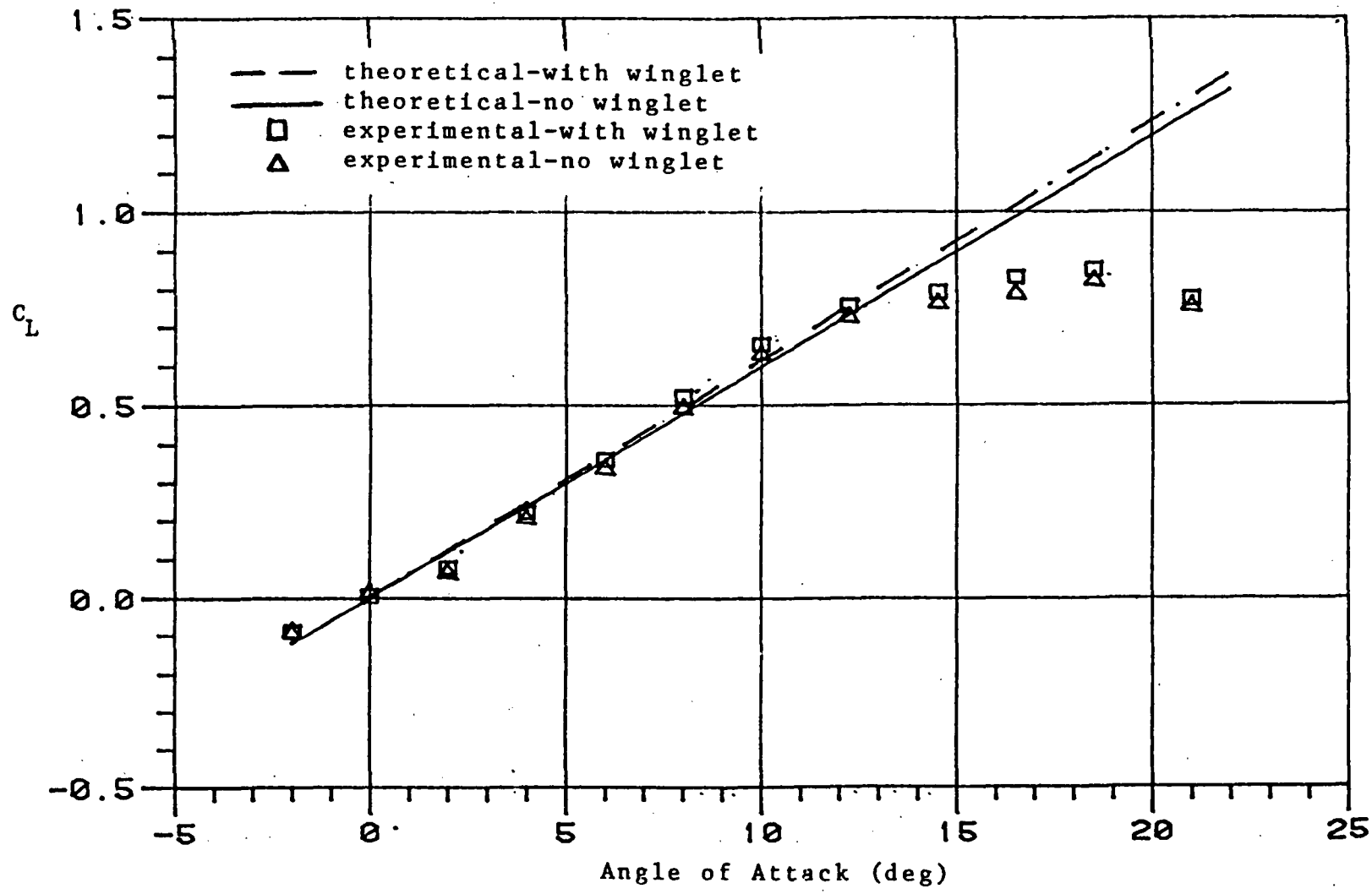

Figure 4-1 Lift Coefficient versus Angle of Attack for the 0 Degree Decalage Configuration

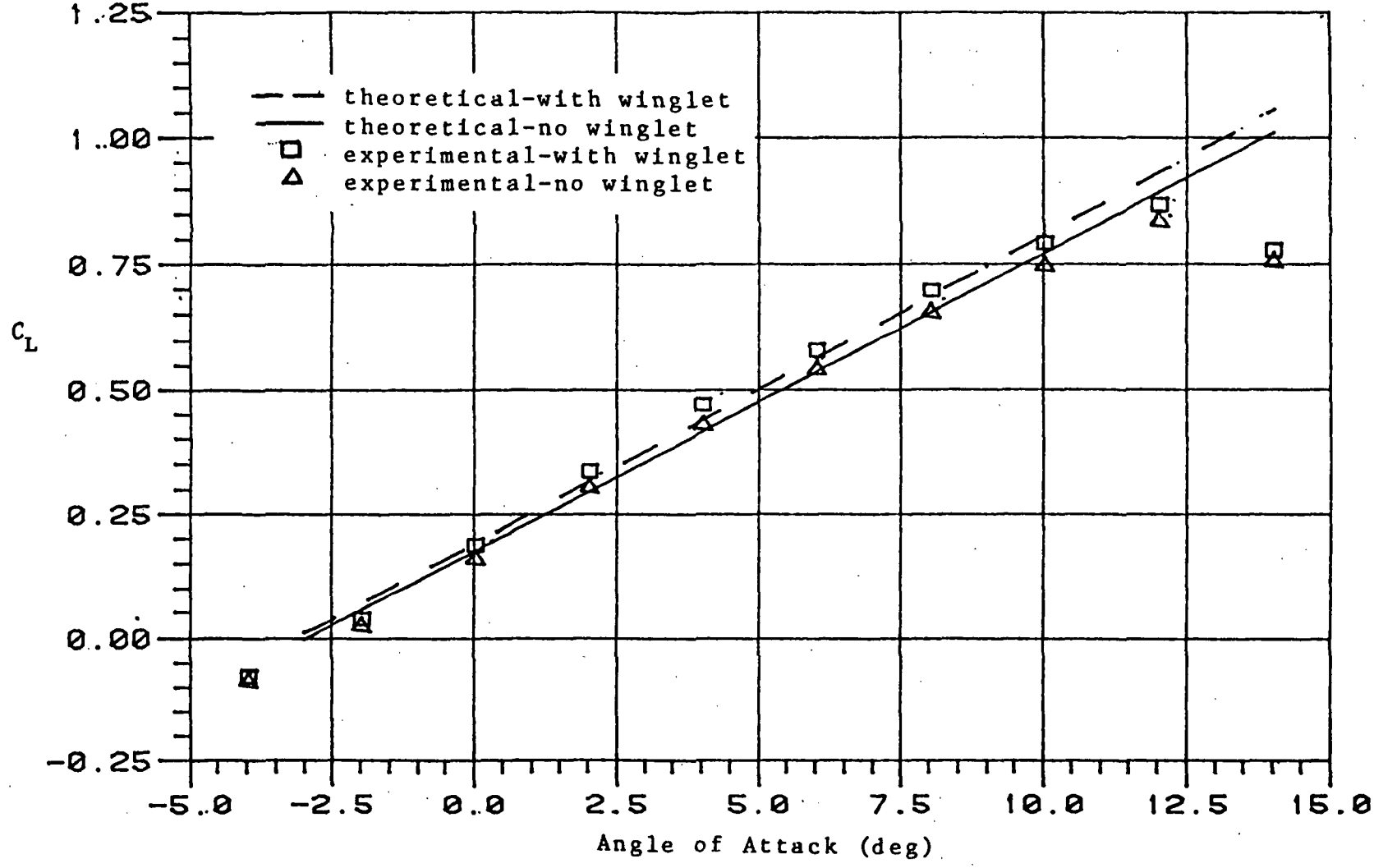

Figure 4-2 Lift Coefficient versus Angle of Attack for the -5 Degree Decalage Configuration

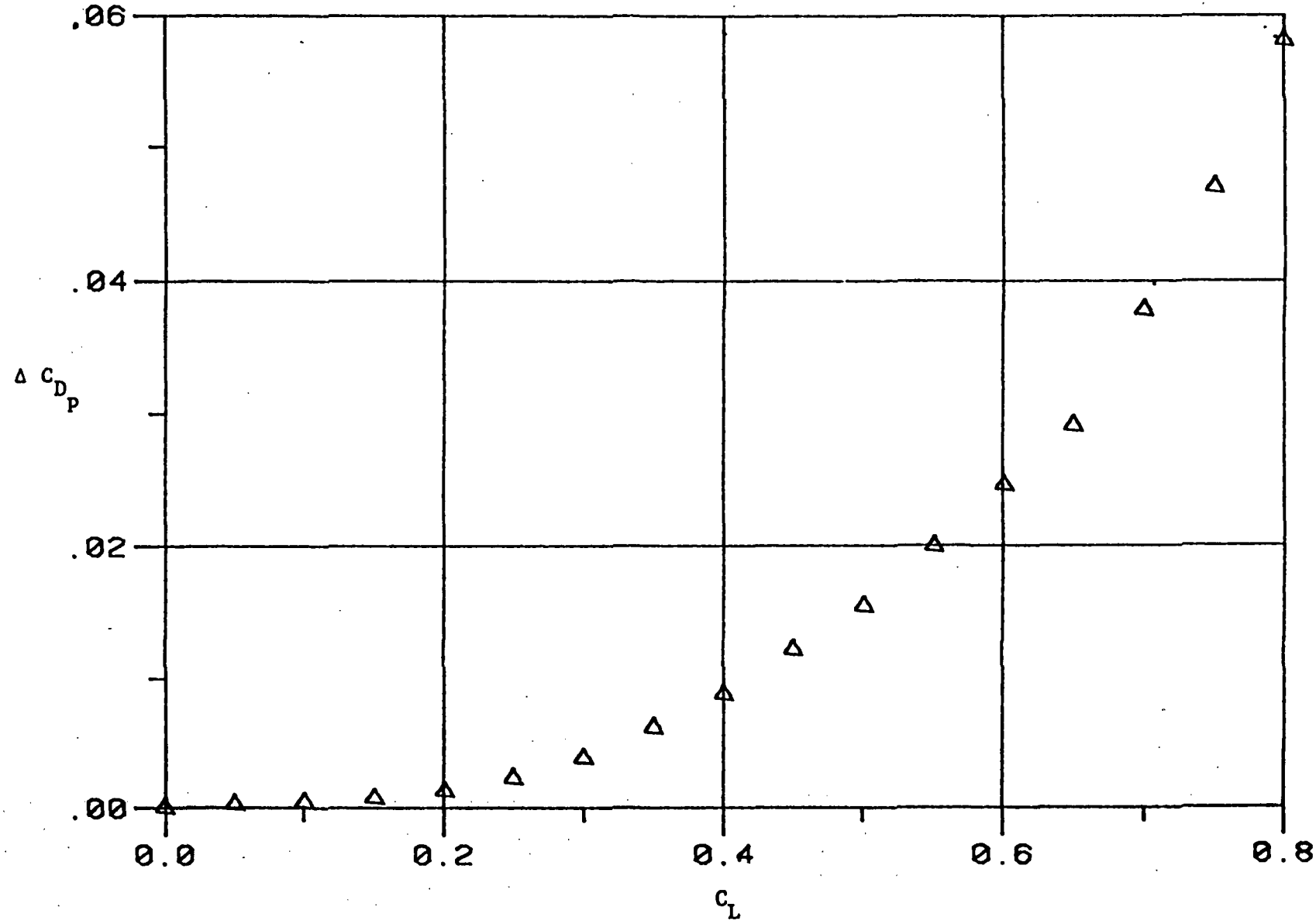

Figure 4-3 Incremental Change in Profile Drag Coefficient as a Function of Lift Coefficient

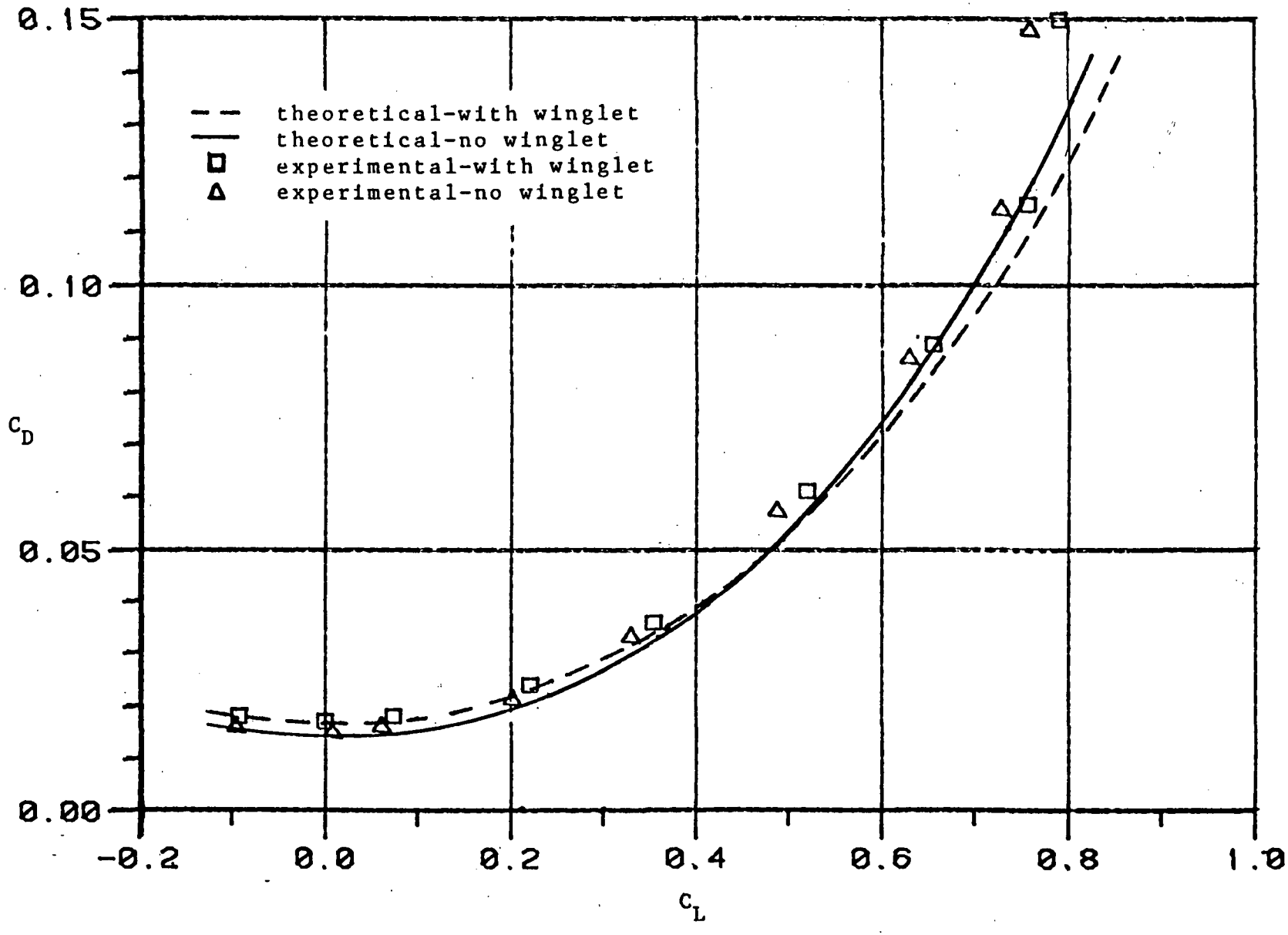

Figure 4-4 Biplane Drag Polar for the 0 Degree Decalage Configuration

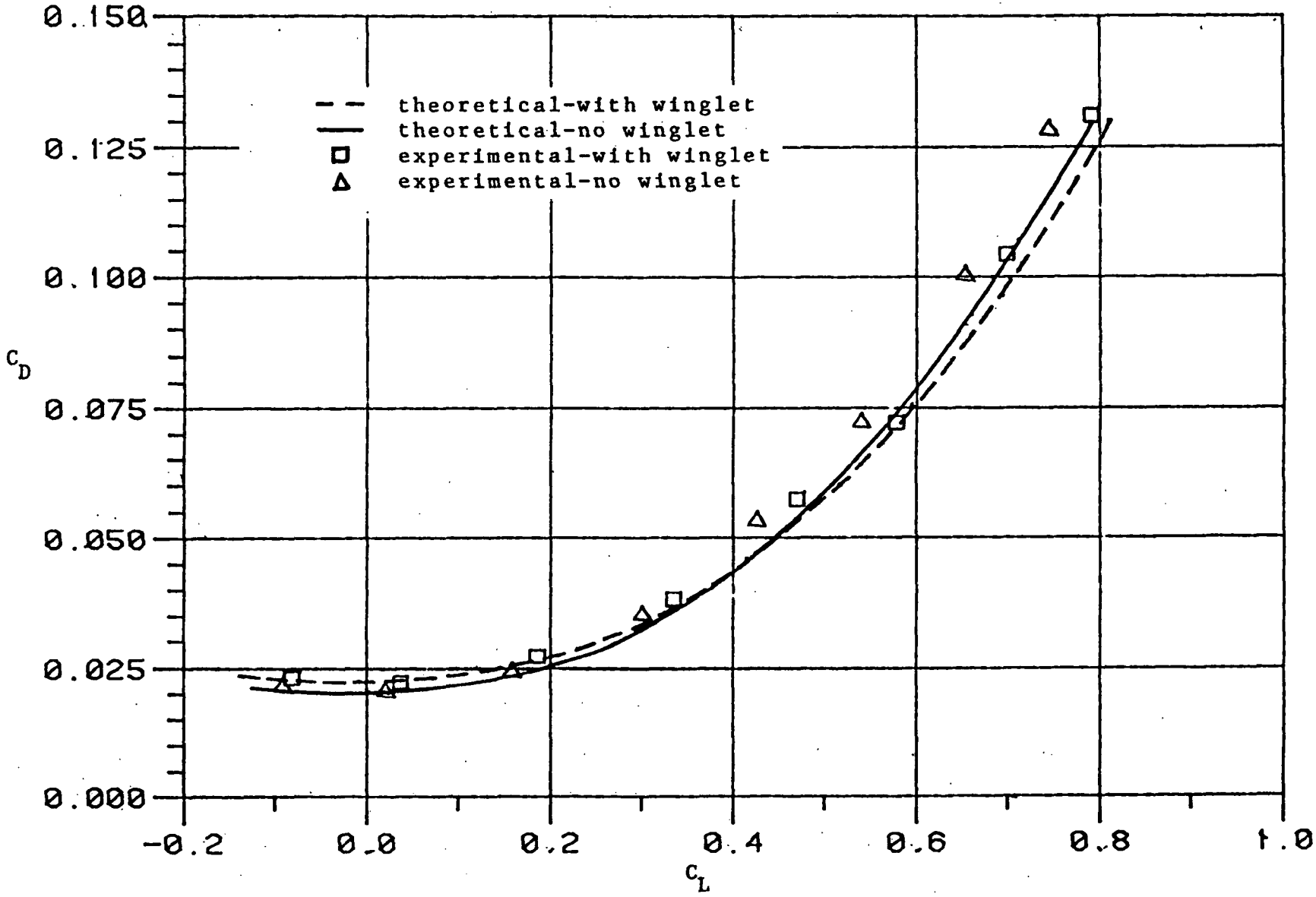

Figure 4-5 Biplane Drag Polar for the -5 Degree Decalage Configuration

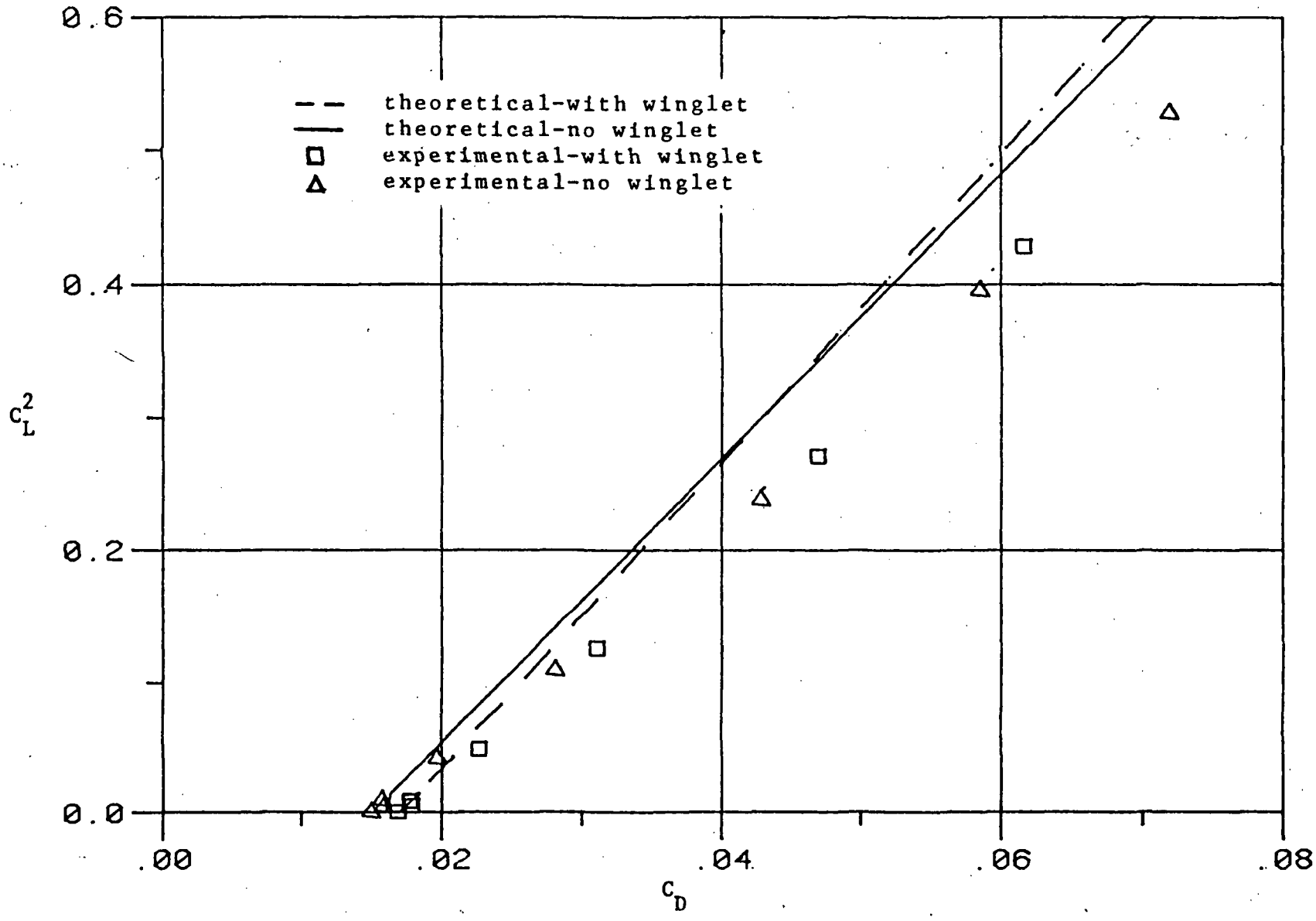

Figure 4-6 Lift Coefficient Squared versus Drag Coefficient for the 0 Degree Decalage Configuration

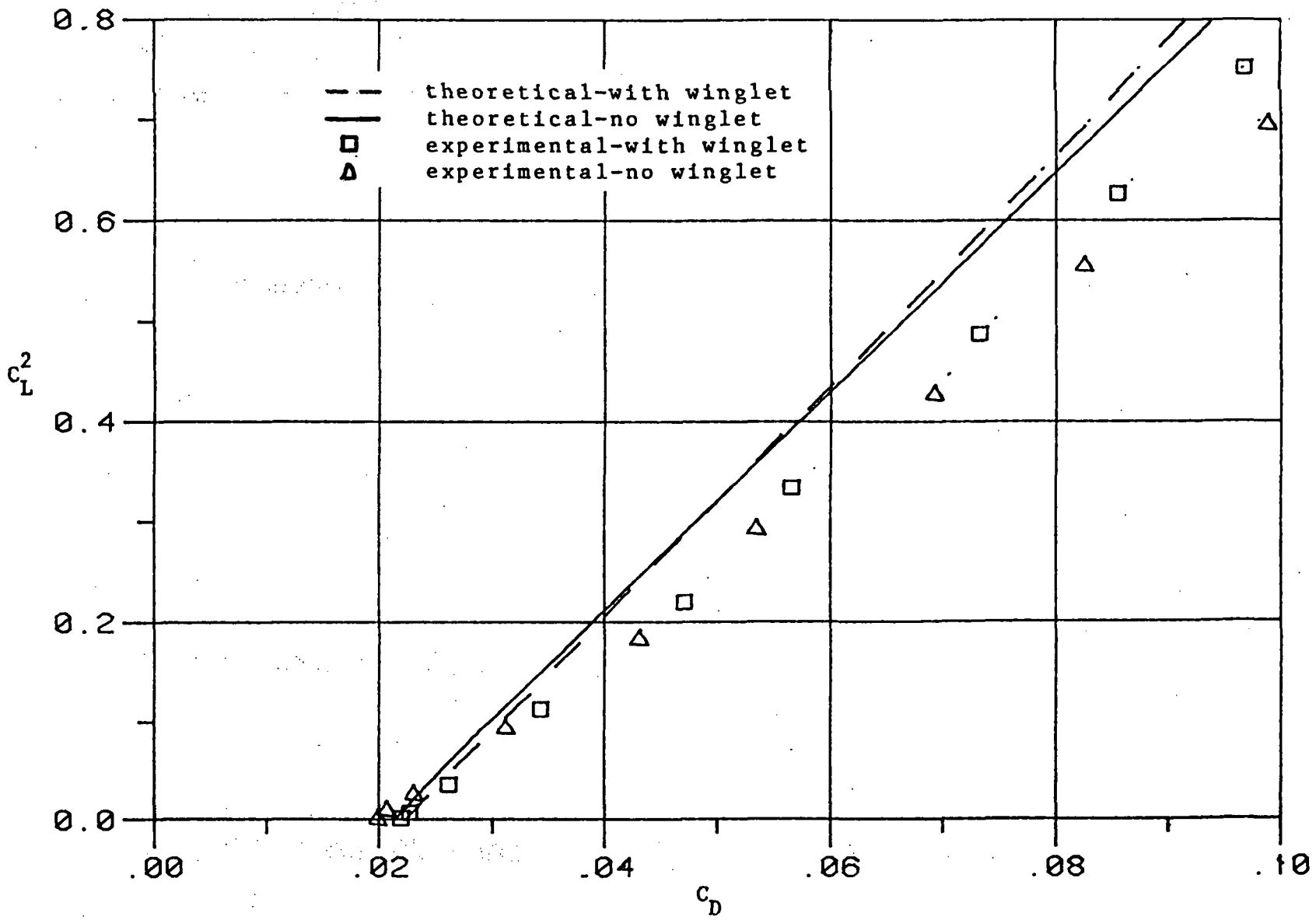

Figure 4-7 Lift Coefficient Squared versus Drag Coefficient for the -5 Degree Decalage Configuration

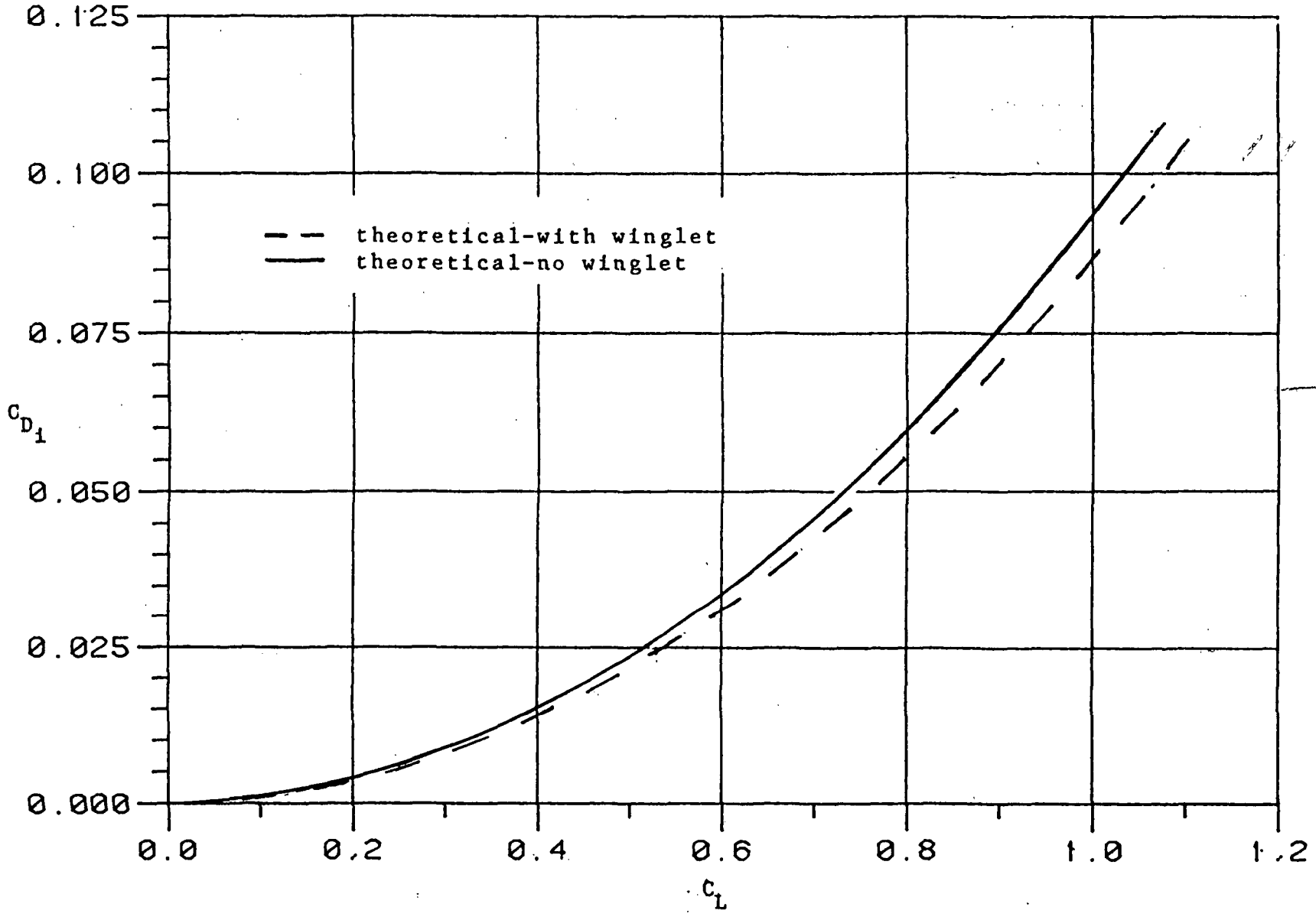

Figure 4-8 Theoretically Predicted Induced Drag Coefficient versus Lift Coefficient for the 0 Degree Decalage Configuration

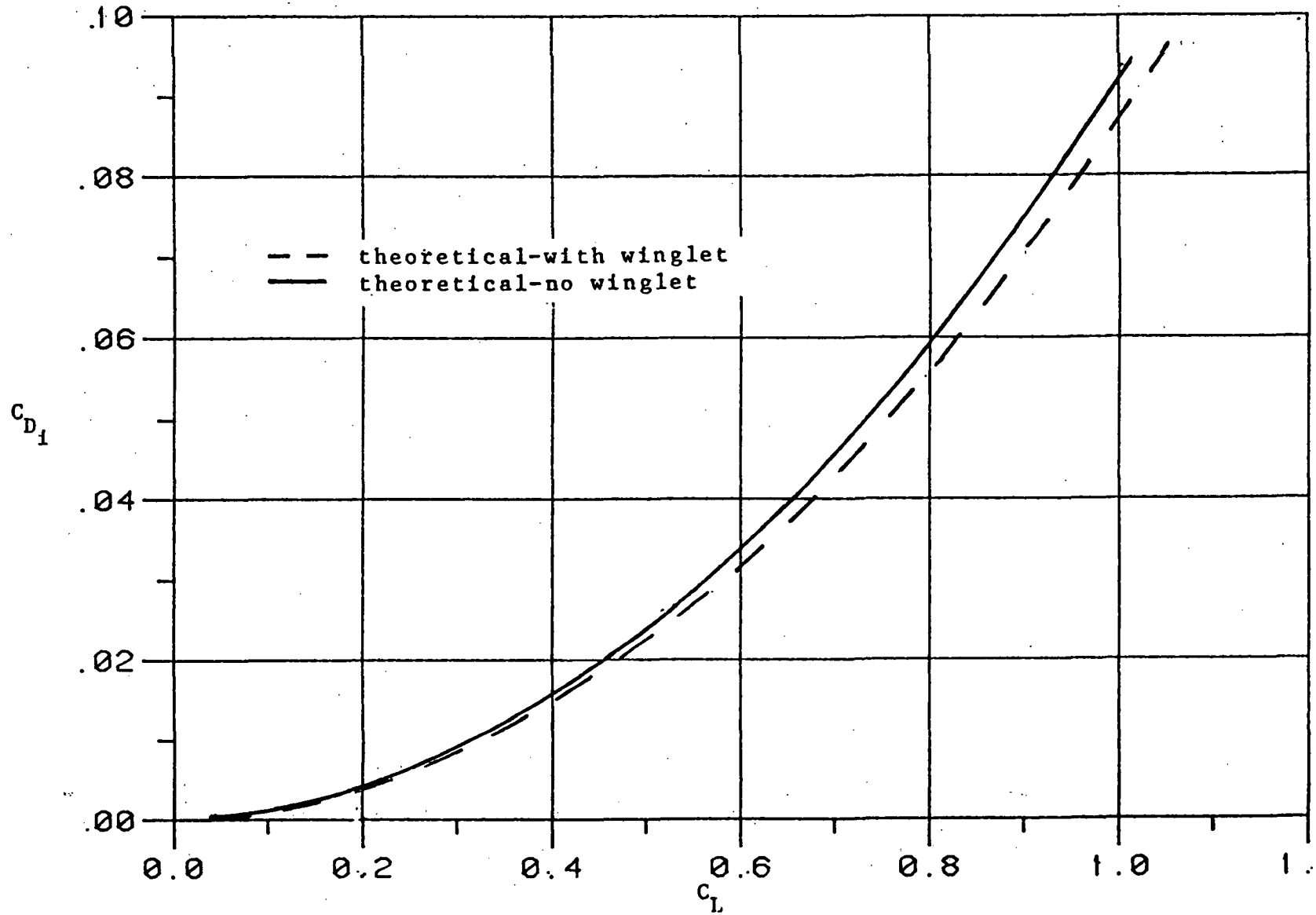

Figure 4-9 Theoretically Predicted Induced Drag Coefficient versus Lift Coefficient for the -5 Degree Decalage Configuration

CHAPTER V

CONCLUSIONS

Based on results determined from the theoretical vortex-lattice computer program and the reduced experimental data collected from wind-tunnel tests conducted at a Reynolds number of 510,000, the following conclusions can can be determined concerning the aerodynamic characteristics of the biplane-winglet configuration.

1. For the 0 degree decalage case, the addition of winglets increased the maximum lift coefficient by 3.6%, increased the lift-curve slope by 5.1%, and (based on experimental data) increased the overall efficiency factor by 13.4%.

2. For the -5 degree decalage case, the addition of winglets increased the maximum lift coefficient by 4.1%, increased the lift-curve slope by 5.3%, and increased the overall efficiency factor by 12.6%

3. The most significant difference between the 0 and -5 degree decalage cases was that the 0 degree decalage case showed a 5% increase in the efficiency factor over the -5 degree decalage case. Also, the -5 degree decalage case showed a

slightly higher maximum lift coefficient.

4. For both configurations, the addition of winglets resulted in approximately a 3.3% reduction in total drag at a lift coefficient of 0.5, and a 6.5% reduction in total drag at a lift coefficient of 0.7. Below a lift coefficient of 0.4, the configurations tested with winglets produced slightly more total drag due to the additional parasite drag created by the winglets (the winglets produced an additional minimum profile drag increment of 0.002).

5. The vortex-lattice computer program results showed a 6.2% reduction in induced drag at a lift coefficient of 0.4, and a 8.3% reduction at a lift coefficient of 0.8. Theoretical results did not indicate any significant differences in induced drag reductions (due to winglets) between the 0 and -5 degree decalage cases.

Overall, it can be determined that the addition of winglets to an already optimized biplane configuration can be beneficial with respect to increasing the maximum lift coefficient, increasing the lift-curve slope, and increasing the overall efficiency of the lifting

system by decreasing the induced drag.

Additional research is suggested to further optimize the biplane-winglet configuration. Possible extensions to the work already done are: varying the winglet airfoil and planform shape, and introducing large winglet cant and toe angles. These new configurations may further optimize the efficiency of the biplane-winglet configuration.

REFERENCES

1. Abbot, Ira H. and Von Doenhoff, Albert E.: "Theory of Wing Sections," McGraw-Hill Book Company, Inc., 1936; New York.

2. Addoms, Robert B. and Spaid, Frank W.: "Aerodynamic Design of High-Performance Biplane Wings," Journal of Aircraft, August 1975.

3. Blackwell, James A., Jr.: "A Finite-Step Method for Calculation of Theoretical Load Distibutions for Arbitrary Lifting-Surface Arrangements at Subsonic Speeds," NASA Technical Note D-5335, 1969.

4. Blackwell, James A.: "Numerical Method to Calculate the Induced Drag or Optimum Loading for Arbitrary Non-Planer Aircraft," Presented at a workshop held at NASA Langley Research Center, Hampton, Virginia, May 17-18, 1976.

5. DeYoung, John: "Historical Evolution of Vortex-Lattice Methods," Presented at a vortex-lattice utilization workshop held at NASA Langley Research Center, Hampton, Virginia, May 17-18, 1976.

6. DeYoung, John: "Induced Drag Ideal Efficiency Factors of Arbitrary Lateral-Vertical Wing Forms," NASA Contractor Report 3357, 1980.

7. Durand, W.F.: "Aerodynamic Theory," Dover Publications, Inc., 1963; New York, Volume II, Division E.

8. Heyson, Harry H.; Riebe, Gregory D.; and Fulton, Cynthia L.: "Theoretical Parametric Study of the Relative Advantages of Winglets and Wing-Tip Extensions," NASA Technical Paper 1020, 1977.

9. Holmes, Bruce J.; VanDam, Cornelis P.; Brown, Philip P.; and Deal, Perry L.: "Flight Evaluation of the Effect of Winglets on Performance and Handling Qualities of a Single-Engine General Aviation Airplane," NASA Technical Memorandum 81892, 1980.

10. Jacobs, Eastman N. and Sherman, Albert: "Airfoil Section Characteristics as Affected by Variations in Reynolds Number," NACA Report Number 586, 1939.

11. Knight, Montgomery and Noyes, Richard W.: "Wind Tunnel Tests on a Series of Biplane Wing Models, Part I. Effects of Changes in Stagger and Gap," NACA Technical Note 310, 1929.

12. Knight, Montgomery and Noyes, Richard W.: "Wind Tunnel Tests on a Series of Biplane Wing Models, Part II. Effects of changes in Decalage, Dihedral, Sweepback, and Overhang," NACA Technical Note 325, 1929.

13. Knight, Montgomery and Noyes, Richard W.: "Wind Tunnel Tests on a Series of Biplane Wing Models, Part III. Effects of Changes in Various Combinations of Stagger, Gap, Decalage, and Sweepback," NACA Technical Note 330, 1929.

14. Lundry, J.L.: "A Numerical Solution for the Minimum Induced Drag and the Corresponding Loading of Non-Planer Wings," NASA Contractor Report 1218, 1968.

15. Margason, Richard J. and Lamar, John E.: "Vortex-Lattice Program for Estimating Subsonic Aerodynamic Characteristics of Complex Planforms," NASA Technical Report D-6142, 1971.

16. Nenadovitch, Miroslave: "Recherches Sur Les Cellules Biplanes Rigides D'Envergure Infine," Publications Scientifigues of Technigues du Ministere de L'Air, Institut Aerotechnigue de Saint-Cyr, Paris, 1936.

17. Norton, F.H.: "The Effect Of Staggering a Biplane," NACA Technical Note 70, 1921.

18. Olson, E.C.: "Experimental Determination of Improved Aerodynamic Characteristics Utilizing Biplane Wing Configurations," M.S. Thesis, University of Missouri-Rolla, Rolla, Missouri, 1974.

19. Pope, Alan: "Wind Tunnel Testing," John Wiley and Sons, Inc.,1947; New York.

20. Von Mises, Richard: "Theory of Flight," McGraw-Hill Book Company, Inc., 1945; New York.

21. Warsaw, Edward P.: "Airplane Design," McGraw-Hill Book Company,Inc., 1936; New York.

22. Whitcomb, Richard T.: "A Design Approach and Selected Wind-Tunnel Results at High Subsonic Speeds for Wing-Tip Mounted Winglets," NASA Technical Note D-8260, 1976.

Appendix

PROGRAM LISTING

```
C     THIS PROGRAM WILL UTILIZE THE VORTEX LATTICE METHOD
C     TO PREDICT THE AERODYNAMIC CHARACTERISTICS OF A
C     BIPLANE-WINGLET CONFIGURATION.
C
C     THE PRIMARY VARIABLES IN THIS PROGRAM WILL BE THE
C     BIPLANE GAP, STAGGER, DECALAGE, SPAN, CHORD, ASPECT
C     RATIO, WINGLET TOE ANGLE (INCIDENCE), WINGLET ASPECT
C     RATIO, AND ANGLE OF ATTACK.
C
C     FOR THIS PARTICULAR CONFIGURATION;
C
C          VEL= FREESTREAM VELOCITY
C          AR=ASPECT RATIO
C          CH=CHORD
C          GAP=GAP(ONE CHORD LENGTH)
C          STAG=STAGGER (IN PERCENT CHORD)
C          DEC=DECALAGE(DEGREES)
C          ALPHU= ANGLE OF ATTACK OF UPPER WING
C          ALPHL= ANGLE OF ATTACK OF LOWER WING
C          TOE=TOE ANGLE OF WINGLET (POSITIVE- TOE INWARD)
C          SW=WING PLANFORM AREA
C
C          N1= NO. OF HORSESHOE VORTICES LOCATED ON UPPER WING (HALF-SPAN)
C          N2= NO. OF HORSESHOE VORTICES LOCATED ON BOTH UPPER
C              AND LOWER WING (HALF-SPAN)
C          N3= NO. OF HORSESHOE VORTICES LOCATED ON BOTH UPPER AND LOWER
C              WING PLUS THE WINGLET (HALF-SPAN)
C
C          PN(N),QN(N),RN(N)= COORDINATES OF THE Nth HORSESHOE VORTEX
C          PV(V),QV(V),RV(V)= COORDINATES OF THE Vth HORSESHOE VORTEX
C
C          S= SEMI-WIDTH OF HORSESHOE VORTEX
C
C
C
      DIMENSION PN(100),QN(100),RN(100),PV(100),QV(100),RV(100)
      DIMENSION FWS(100,100),FWP(100,100),FVS(100,100),FVP(100,100)
      DIMENSION GAM(100),WKAREA(100),A(100,100),ALPH(100),B(100)
      DIMENSION PH(100),WW(100),WWL(100),VW(100),VWL(100),TOE(100)
```

```
      DIMENSION SEC(100)

      INTEGER V,V1,V2,V3,V4,V5,V6,IA,IDGT

      PI=3.141592

      VEL=100.0
C
C       **** INPUT BIPLANE-WINGLET GEOMETRY ****

      WRITE(6,*)'ENTER WING TWIST'
      READ(5,*)EW
      WRITE(6,*)'ENTER ASPECT RATIO'
      READ(5,*)AR
      WRITE(6,*)'ENTER BIPLANE STAGGER'
      READ(5,*)STAG
      WRITE(6,*)'ENTER ALPHA (UPPER WING)'
      READ(5,*)ALPHU
      WRITE(6,*)'ENTER BIPLANE DECALAGE'
      READ(5,*)DEC



      WRITE(6,*)'ENTER WINGLET MAXIMUM TOE ANGLE'
      READ(5,*)ALPHI

      BB=20.0
      CH=BB/AR
      GAP=CH
      ALPHL=ALPHU-DEC

      S=0.25

      N1=20
      N2=40
      N3=60
      N4=80
      N5=88
      N6=96
```

```
      V1=20
      V2=40
      V3=60
      V4=80
      V5=88
      V6=96

      KN=2
      K=8


      WRITE(8,200)N6,BB,AR,ALPHU,DEC,STAG,CH,ALPHI
  200  FORMAT(//,2X,'TOTAL NUMER OF HORSESHOE VORTICES =',I4,//,2X,'SPA
     @N =',F4.1,25X,'ASPECT RATIO =',F6.2,15X,//,2X,'ALPHA UPPER =',
     @F4.1,15X,'   DECALAGE =',F4.1,//,2X,'STAGGER =',F4.1,
     @22X,'CHORD =',F4.1,//,2X,'MAXIMUM WINGLET TOE ANGLE =',F4.1)
C
C
C      **** COMPUTE ARRAY OF COORDINATES FOR THE Nth HORSESHOE VORTEX ****
C
C
      DO 5 V=1,N6
      DO 10 N=1,N6
         IF(N.LE.N1) THEN
           PN(N)=-(CH/K)
           QN(N)=(2.*FLOAT(N)-1.)*S
           RN(N)=0.0
           PH(N)=0.0
         ELSE IF(N.LE.N2) THEN
           PN(N)=-(5.*CH/K)
           QN(N)=( 2.*(FLOAT(N)-N1)-1.)*S
           RN(N)=0.0
           PH(N)=0.0
         ELSE IF(N.LE.N3) THEN
           PN(N)=-(STAG*CH)-(CH/K)
           QN(N)=(2.*(N-N2)-1.)*S
           RN(N)=GAP
           PH(N)=0.0
```

```
      ELSE IF(N.LE.N4)THEN
        PN(N)=-(STAG*CH)-(5*CH/K)
        QN(N)=(2.*(N-N3)-1.)*S
        RN(N)=GAP
        PH(N)=0.0
      ELSE IF(N.LE.N5)THEN
        PN(N)=-(STAG*CH/(2.*K))*(2.*(N-N4)-1.)-(CH/K)
        QN(N)=BB/2.



        RN(N)=(2.*(N-N4)-1.)*(CH/16.)
        PH(N)=PI/2.
      ELSE IF(N.LE.N6)THEN
        PN(N)=-(STAG*CH/(2.*K))*(2.*(N-N5)-1.)-(5.*CH/K)
        QN(N)=BB/2.
        RN(N)=(2.*(N-N5)-1.)*(CH/16.)
        PH(N)=PI/2.
      END IF

C      **** COMPUTE ARRAY OF COORDINATES FOR THE Vth CONTROL POINT ****

      IF(V.LE.V1) THEN
        PV(V)=-(3.*CH/K)
        QV(V)=(2.*FLOAT(V)-1.)*S
        RV(V)=0.0
        ALPH(V)=ALPHU
      ELSE IF(V.LE.V2) THEN
        PV(V)=-(7.*CH/K)
        QV(V)=(2.*(FLOAT(V)-V1)-1.)*S
        RV(V)=0.0
        ALPH(V)=ALPHU
      ELSE IF(V.LE.V3) THEN
        PV(V)=-(STAG*CH)-(3.*CH/K)
        QV(V)=(2.*(V-V2)-1.)*S
        RV(V)=GAP
        ALPH(V)=ALPHL
      ELSE IF(V.LE.V4)THEN
```

```
          PV(V)=-(STAG*CH)-(7.*CH/K)
          QV(V)=(2.*(V-V3)-1.)*S
          RV(V)=GAP
          ALPH(V)=ALPHL
        ELSE IF(V.LE.V5)THEN
          PV(V)=-(STAG*CH/(2.*K))*(2.*(V-V4)-1.)-(3.*CH/K)
          QV(V)=BB/2.
          RV(V)=(2.*(V-V4)-1.)*(CH/16.)
          TOE(V)=(GAP/2.-RV(V))*(2.*(ALPHI/GAP))
        ELSE IF(V.LE.V6)THEN
          PV(V)=-(STAG*CH/(2.*K))*(2.*(V-V5)-1.)-(7.*CH/K)
          QV(V)=BB/2.
          RV(V)=(2.*(V-V5)-1.)*(CH/16.)
          TOE(V)=(GAP/2.-RV(V))*(2.*(ALPHI/GAP))
        END IF


        X=PV(V)-PN(N)
        YS=QV(V)-QN(N)
        YP=QV(V)+QN(N)
        Z=RV(V)-RN(N)
        PHS=PH(N)
        PHP=-PH(N)

C
C   *** COMPUTE DOWNWASH INFLUENCE COEFFICIENTS AT CONTROL POINTS ON WINGS***
C
C
C   **** DOWNWASH COEFFICIENT- STARBOARD WING ***
C
        CALL FWSS(FWS,N,V,X,YS,Z,S,PHS,WS1,WS2,WS3,WS4,WS5,WS7,WS9)
C
C   **** DOWNWASH COEFFICIENT- PORT WING ****
C
        CALL FWPP(FWP,N,V,X,YP,Z,S,PHP,WP1,WP2,WP3,WP4,WP5,WP7,WP9)
C
```

```
C    *** COMPUTE SIDEWASH COEFICIENTS AT CONTROL POINTS ON WINGLETS ***
C
C
C    **** SIDEWASH COEFFICIENT- STARBOARD WINGLET ****
C
       CALL FVSS(FVS,N,V,X,YS,Z,S,PHS,WS1,WS2,WS3,WS4,WS5,WS7,WS9)
C
C    **** SIDEWASH COEFFICIENT- PORT WINGLET ****

C
       CALL FVPP(FVP,N,V,X,YP,Z,S,PHP,WP1,WP2,WP3,WP4,WP5,WP7,WP9)
C
C
C     *** CALCULATE COEFFICIENT MATRIX FOR CONTROL POINTS LOCATED ***
C     *** ON UPPER AND LOWER WINGS                                ***
C
C
       IF(V.GT.V4)GO TO 100
         A(V,N)=FWP(V,N)+FWS(V,N)
         B(V)=4.*PI*VEL*ALPH(V)*(PI/180.)
       GO TO 10
C
C     *** CALCULATE COEFFICIENT MATRIX FOR CONTROL POINTS ON WINGLETS ***
C
  100    A(V,N)=FVP(V,N)+FVS(V,N)
         B(81)=4.*PI*VEL*TOE(81)*(PI/180.)
         B(82)=4.*PI*VEL*TOE(82)*(PI/180.)
         B(83)=4.*PI*VEL*TOE(83)*(PI/180.)
         B(84)=4.*PI*VEL*TOE(84)*(PI/180.)
         B(85)=4.*PI*VEL*TOE(85)*(PI/180.)
         B(86)=4.*PI*VEL*TOE(86)*(PI/180.)
         B(87)=4.*PI*VEL*TOE(87)*(PI/180.)
         B(88)=4.*PI*VEL*TOE(88)*(PI/180.)
         B(89)=B(81)
         B(90)=B(82)
         B(91)=B(83)
         B(92)=B(84)
         B(93)=B(85)
```

```
          B(94)=B(86)
          B(95)=B(87)
          B(96)=B(88)

   10     CONTINUE
    5     CONTINUE

C
C       *** PROGRAM IS NOW READY TO SOLVE FOR THE GAMMA ARRAY FROM THE ***
C       *** COEFFICIENT MATRIX AND THE BOUNDRY CONDITION ARRAY          ***
C

        M=1
        N=N6
        IA=100
        IDGT=6
C
C       *** CALL IMSL SUBROUTINE TO SOLVE N SIMULTANIOUS EQUATIONS ***
C
        CALL LEQT1F(A,M,N,IA,B,IDGT,WKAREA,IER)

        DO 15 V=1,N6
        GAM(V)=B(V)
   15   CONTINUE




C
C       *** CALCULATE LIFT COEFFICIENTS FOR UPPER AND LOWER WINGS ***
C
        CLUPP=0.0
        CLLOW=0.0

        ST=2.*(BB*CH)
        SW=BB*CH

          DO 20 V=1,20
```

```
          CLUPP=CLUPP+(4./(VEL*SW))*((GAM(V)+GAM(V+20))*2.0*S)
          SEC(V)=(2.*(GAM(V)+GAM(V+20)))/(CH*VEL)

110       CLLOW=CLLOW+(4./(VEL*SW))*((GAM(V+40)+GAM(V+60))*2.0*S)
          SEC(V+20)=(2.*(GAM(V+40)+GAM(V+60)))/(CH*VEL)
20     CONTINUE

       DO 21 V=81,V5
          SEC(V)=(2.*(GAM(V)+GAM(V+8)))/(CH*VEL)
21     CONTINUE

        CL=(CLUPP+CLLOW)/2.

      WRITE(8,189)
189   FORMAT(/,5X,'CONTROL POINT',5X,'SECTION LIFT COEFF',3X,'SECTION
     @LIFT COEFF',/,27X,'UPPER WING',9X,'LOWER WING',/)

      DO 16 V=1,20
      WRITE(8,190)V,SEC(V),SEC(V+20)
190   FORMAT(10X,I3,12X,F9.5,10X,F9.5)
 16   CONTINUE

      WRITE(8,188)
188   FORMAT(//,5X,'CONTROL POINT',10X,'WINGLET SECTION LIFT COEFF',/)

      DO 17 V=81,V5
      WRITE(8,187)V,SEC(V)
187   FORMAT(10X,I3,22X,F9.5)
 17   CONTINUE

      WRITE(8,202)CLUPP,CLLOW,CL
202   FORMAT(//,5X,'LIFT COEFF (UPPER WING) =',F10.6,
     @/,5X,'LIFT COEFF (LOWER WING) =',F10.6,
     @/,5X,'TOTAL LIFT COEFF =       ',F10.6)
C
C
C    **** CALCULATION OF INDUCED DRAG BY MUNK'S THEOREM OF INDUCED ****
C    ****      DRAG DETERMINATION UTILIZING THE TREFFTZ PLANE       ****
C
C
```

```
      TREF=-1400.0

    DO 50 V=1,V6
    DO 55 N=1,N6
      X=TREF
      YS=QV(V)-QN(N)
      YP=QV(V)+QN(N)
      Z=RV(V)-RN(N)
      PHS=PH(N)
      PHP=-PH(N)

      CALL FWSS(FWS,N,V,X,YS,Z,S,PHS,WS1,WS2,WS3,WS4,WS5,WS7,WS9)



      CALL FWPP(FWP,N,V,X,YP,Z,S,PHP,WP1,WP2,WP3,WP4,WP5,WP7,WP9)
      CALL FVSS(FVS,N,V,X,YS,Z,S,PHS,WS1,WS2,WS3,WS4,WS5,WS7,WS9)
      CALL FVPP(FVP,N,V,X,YP,Z,S,PHP,WP1,WP2,WP3,WP4,WP5,WP7,WP9)
 55   CONTINUE
 50   CONTINUE
C
C
C   **** CALCULATION OF INDUCED VELOCITYS IN THE TREFFTZ PLANE ****
C
C

    ROW=0.002378

    DO 60 V=1,96


      WW(V)=0.0
      WWL(V)=0.0
      VW(V)=0.0
      VWL(V)=0.0

      DO 65 N=1,80

        IF(V.LE.80)THEN
         WW(V)=(GAM(N)/(4.*PI))*(FWP(V,N)+FWS(V,N))+WW(V)
```

```
            ELSE IF(V.LE.96)THEN
             VW(V)=(GAM(N)/(4.*PI))*(FVP(V,N)+FVS(V,N))+VW(V)
            END IF

 65       CONTINUE

          DO 70 N=81,96

            IF(V.LE.80)THEN
             WWL(V)=(GAM(N)/(4.*PI))*(FWP(V,N)+FWS(V,N))+WWL(V)
            ELSE IF(V.LE.96)THEN
             VWL(V)=(GAM(N)/(4.*PI))*(FVP(V,N)+FVS(V,N))+VWL(V)
            END IF

 70       CONTINUE

 60    CONTINUE

C
C
C   *** CALCULATION OF INDUCED DRAG CREATED BY UPPER AND LOWER WINGS ***
C
C
      DWW=0.0
      DWWL=0.0
      DVW=0.0
      DVWL=0.0


      DO 75 V=1,80
         N=V
         DWW=ROW*2.*S*WW(V)*GAM(N)+DWW
         DWWL=ROW*2.*S*WWL(V)*GAM(N)+DWWL
 75    CONTINUE
C
C
C      *** CALCULATION OF INDUCED DRAG CREATED BY WINGLETS ***
C
```

```
      DO 80 V=81,96
         N=V
         DVW=-ROW*2.*S*VW(V)*GAM(N)+DVW
         DVWL=-ROW*2.*S*VWL(V)*GAM(N)+DVWL
 80   CONTINUE

C
C
C     *** CALCULATION OF DRAG COEFFICIENTS FOR WINGS AND WINGLETS ***
C
C
      Q=0.5*ROW*(VEL**2.)
        CDWW=DWW/(Q*ST)
        CDWWL=DWWL/(Q*ST)
        CDVW=DVW/(Q*ST)
        CDVWL=DVWL/(Q*ST)
        CDW=CDWW+CDWWL
        CDWL=CDVW+CDVWL
        CD=CDW+CDWL
        E=(CL**2.0)/(PI*AR*CD)
        CLALPH=CL/(ALPHU-(DEC/1.667))
        RLD=CL/CD

      WRITE(8,203)CDWW,CDWWL,CDVW,CDVWL,CDW,CDWL,CD,E,CLALPH,RLD
 203  FORMAT(//,5X,'DRAG COEFF(WING-WING)=',F16.6,
     @/,5X,'DRAG COEFF(WING-WINGLET)=',F13.6,
     @/,5X,'DRAG COEFF(WINGLET-WING)=',F13.6,
     @/,5X,'DRAG COEFF(WINGLET-WINGLET)=',F10.6,
     @//,5X,'TOTAL WING DRAG COEFF=',F13.6,
     @/,5X,'TOTAL WINGLET DRAG COEFF=',F10.6,
     @/,5X,'TOTAL BIPLANE DRAG COEFF=',F10.6,
     @//,5X,'OSWALDS EFFICIENCY FACTOR=',F10.6,
     @/,5X,'3-D LIFT SLOPE CURVE(/DEG)=',F9.6,
     @/,5X,'LIFT/DRAG RATIO(W/ CDmin)= ',F9.6)
```

```
C    ***** THE FOLLOWING SECTION OF THIS PROGRAM WILL COMPUTE THE *****
C    *                                                               *
C    ***** AERODYNAMIC CHACTERISTICS OF THE BIPLANE CONFIGURATION *****
C    *                                                               *
C    ********************* WITH NO WINGLETS ****************************


      DO 6 V=1,N4
      DO 11 N=1,N4

         X=PV(V)-PN(N)
         YS=QV(V)-QN(N)
         YP=QV(V)+QN(N)
         Z=RV(V)-RN(N)
         PHS=PH(N)
         PHP=-PH(N)
C
C
C
C    *** COMPUTE DOWNWASH INFLUENCE COEFFICIENTS AT CONTROL POINTS ON WINGS***
C
C
C    **** DOWNWASH COEFFICIENT- STARBOARD WING ***
C


      CALL FWSS(FWS,N,V,X,YS,Z,S,PHS,WS1,WS2,WS3,WS4,WS5,WS7,WS9)
C
C    **** DOWNWASH COEFFICIENT- PORT WING ****
C
      CALL FWPP(FWP,N,V,X,YP,Z,S,PHP,WP1,WP2,WP3,WP4,WP5,WP7,WP9)
C
C
C
C     *** CALCULATE COEFFICIENT MATRIX FOR CONTROL POINTS LOCATED ***
C     *** ON UPPER AND LOWER WINGS                                ***
```

```
C
        A(V,N)=FWP(V,N)+FWS(V,N)
        B(V)=4.*PI*VEL*ALPH(V)*(PI/180.)

   11   CONTINUE
    6   CONTINUE
C
C     *** PROGRAM IS NOW READY TO SOLVE FOR THE GAMMA ARRAY FROM THE ***
C     *** COEFFICIENT MATRIX AND THE BOUNDRY CONDITION ARRAY          ***
C

      M=1
      N=N4
      IA=100
      IDGT=6
C
C     *** CALL IMSL SUBROUTINE TO SOLVE N SIMULTANIOUS EQUATIONS ***
C
      CALL LEQT1F(A,M,N,IA,B,IDGT,WKAREA,IER)

      DO 26 V=1,N4
      GAM(V)=B(V)
 26   CONTINUE

C
C     *** CALCULATE LIFT COEFFICIENTS FOR UPPER AND LOWER WINGS ***
C
      CLUPP=0.0
      CLLOW=0.0

      ST=2.*(BB*CH)
      SW=BB*CH

        DO 22 V=1,20

          CLUPP=CLUPP+(4./(VEL*SW))*((GAM(V)+GAM(V+20))*2.0*S)
          SEC(V)=(2.*(GAM(V)+GAM(V+20)))/(CH*VEL)

          CLLOW=CLLOW+(4./(VEL*SW))*((GAM(V+40)+GAM(V+60))*2.0*S)
```

```
          SEC(V+20)=(2.*(GAM(V+40)+GAM(V+60)))/(CH*VEL)
22      CONTINUE

        CL=(CLUPP+CLLOW)/2.

      WRITE(8,149)
149   FORMAT(///,'TOTAL NUMBER OF HORSESHOE VORTICES =',I4,5X,
     @'NO WINGLETS!',//)
      WRITE(8,150)
150   FORMAT(/,5X,'CONTROL POINT',5X,'SECTION LIFT COEFF',3X,'SECTION
     @LIFT COEFF',/,27X,'UPPER WING',9X,'LOWER WING',/)

      DO 27 V=1,20
      WRITE(8,151)V,SEC(V),SEC(V+20)



151   FORMAT(10X,I3,12X,F9.5,10X,F9.5)
 27   CONTINUE


      WRITE(8,152)CLUPP,CLLOW,CL
152   FORMAT(//,5X,'LIFT COEFF (UPPER WING) =',F10.6,
     @/,5X,'LIFT COEFF (LOWER WING) =',F10.6,
     @/,5X,'TOTAL LIFT COEFF =       ',F10.6)
C
C
C    **** CALCULATION OF INDUCED DRAG BY MUNK'S THEOREM OF INDUCED ****
C    ****      DRAG DETERMINATION UTILIZING THE TREFFTZ PLANE       ****
C
C
C
        TREF=-1400.0

      DO 51 V=1,V4
      DO 56 N=1,N4

        X=TREF
        YS=QV(V)-QN(N)
        YP=QV(V)+QN(N)
```

```
        Z=RV(V)-RN(N)
        PHS=PH(N)
        PHP=-PH(N)

        CALL FWSS(FWS,N,V,X,YS,Z,S,PHS,WS1,WS2,WS3,WS4,WS5,WS7,WS9)
        CALL FWPP(FWP,N,V,X,YP,Z,S,PHP,WP1,WP2,WP3,WP4,WP5,WP7,WP9)
        CALL FVSS(FVS,N,V,X,YS,Z,S,PHS,WS1,WS2,WS3,WS4,WS5,WS7,WS9)
        CALL FVPP(FVP,N,V,X,YP,Z,S,PHP,WP1,WP2,WP3,WP4,WP5,WP7,WP9)

 56   CONTINUE
 51   CONTINUE
C
C
C    **** CALCULATION OF INDUCED VELOCITYS IN THE TREFFTZ PLANE ****
C
C
      ROW=0.002378

      DO 61 V=1,80

         WW(V)=0.0
         WWL(V)=0.0
         VW(V)=0.0
         VWL(V)=0.0

         DO 66 N=1,80

           IF(V.LE.80)THEN
            WW(V)=(GAM(N)/(4.*PI))*(FWP(V,N)+FWS(V,N))+WW(V)
           ELSE IF(V.LE.96)THEN
            VW(V)=(GAM(N)/(4.*PI))*(FVP(V,N)+FVS(V,N))+VW(V)
           END IF

 66      CONTINUE

 61   CONTINUE
C
C
C
```

```
C   *** CALCULATION OF INDUCED DRAG CREATED BY UPPER AND LOWER WINGS ***
C



C
      DWW=0.0
      DWWL=0.0
      DVW=0.0
      DVWL=0.0


      DO 76 V=1,80
         N=V
         DWW=ROW*2.*S*WW(V)*GAM(N)+DWW
         DWWL=ROW*2.*S*WWL(V)*GAM(N)+DWWL
 76   CONTINUE


C
C
C     *** CALCULATION OF DRAG COEFFICIENTS FOR WING ***
C
C

      Q=0.5*ROW*(VEL**2.)
        CDWW=DWW/(Q*ST)
        CDWWL=DWWL/(Q*ST)
        CDVW=DVW/(Q*ST)
        CDVWL=DVWL/(Q*ST)
        CDW=CDWW+CDWWL
        CDWL=CDVW+CDVWL
        CD=CDW+CDWL
        E=(CL**2.0)/(PI*AR*CD)
        CLALPH=CL/(ALPHU-(DEC/1.667))
        RLD=CL/CD

      WRITE(8,154)CDWW,CDWWL,CDVW,CDVWL,CDW,CDWL,CD,E,CLALPH,RLD
 154  FORMAT(//,5X,'DRAG COEFF(WING-WING)=',F16.6,
     @/,5X,'DRAG COEFF(WING-WINGLET)=',F13.6,
```

```
     @/,5X,'DRAG COEFF(WINGLET-WING)=',F13.6,
     @/,5X,'DRAG COEFF(WINGLET-WINGLET)=',F10.6,
     @//,5X,'TOTAL WING DRAG COEFF=',F13.6,
     @/,5X,'TOTAL WINGLET DRAG COEFF=',F10.6,
     @/,5X,'TOTAL BIPLANE DRAG COEFF=',F10.6,
     @//,5X,'OSWALDS EFFICIENCY FACTOR=',F10.6,
     @/,5X,'3-D LIFT SLOPE CURVE(/DEG)=',F9.6,
     @/,5X,'LIFT/DRAG RATIO(W/ CDmin)= ',F9.6)


1000  STOP
      END



C    ************** SUBROUTINE FWS ***************
C    *                                           *
C    *** DOWNWASH COEFFICIENT- STARBOARD WING ***
C
      SUBROUTINE FWSS(FWS,N,V,X,YS,Z,S,PHS,WS1,WS2,WS3,WS4,WS5,WS7,WS9)
        DIMENSION FWS(100,100)
        INTEGER V
        WS1=(-X*COS(PHS))/((X**2.)+((Z*COS(PHS)-YS*SIN(PHS))**2.))
        WS2=((YS+S*COS(PHS))*COS(PHS))+((Z+S*SIN(PHS))*SIN(PHS))
        WS3=((X**2.)+(YS+S*COS(PHS))**2.+(Z+S*SIN(PHS))**2.)**0.5
        WS4=((YS-S*COS(PHS))*COS(PHS))+((Z-S*SIN(PHS))*SIN(PHS))
        WS5=((X**2.)+(YS-S*COS(PHS))**2.+(Z-S*SIN(PHS))**2.)**0.5
        WS6=(YS-S*COS(PHS))/((YS-S*COS(PHS))**2.+(Z-S*SIN(PHS))**2.)
        WS7=1.-(X/WS5)



        WS8=(YS+S*COS(PHS))/((YS+S*COS(PHS))**2.+(Z+S*SIN(PHS))**2.)
        WS9=1.-(X/WS3)

         FWS(V,N)=WS1*(WS2/WS3-WS4/WS5)-(WS6*WS7)+(WS8*WS9)
      RETURN
      END
C
```

```
C     ************ SUBROUTINE FWP ***********
C     *                                     *
C     *** DOWNWASH COEFFICIENT- PORT WING ***
C
      SUBROUTINE FWPP(FWP,N,V,X,YP,Z,S,PHP,WP1,WP2,WP3,WP4,WP5,WP7,WP9)
        DIMENSION FWP(100,100)
        INTEGER V
        WP1=(-X*COS(PHP))/((X**2.)+((Z*COS(PHP)-YP*SIN(PHP))**2.))
        WP2=((YP+S*COS(PHP))*COS(PHP))+((Z+S*SIN(PHP))*SIN(PHP))
        WP3=((X**2.)+(YP+S*COS(PHP))**2.+(Z+S*SIN(PHP))**2.)**0.5
        WP4=((YP-S*COS(PHP))*COS(PHP))+((Z-S*SIN(PHP))*SIN(PHP))
        WP5=((X**2.)+(YP-S*COS(PHP))**2.+(Z-S*SIN(PHP))**2.)**0.5
        WP6=(YP-S*COS(PHP))/((YP-S*COS(PHP))**2.+(Z-S*SIN(PHP))**2.)
        WP7=1.-(X/WP5)
        WP8=(YP+S*COS(PHP))/((YP+S*COS(PHP))**2.+(Z+S*SIN(PHP))**2.)
        WP9=1.-(X/WP3)

        FWP(V,N)=WP1*(WP2/WP3-WP4/WP5)-(WP6*WP7)+(WP8*WP9)
       RETURN
       END
C
C     ************ SUBROUTINE FVS ******************
C     *                                            *
C     *** SIDEWASH COEFFICIENT- STARBOARD WINGLET ***
C
      SUBROUTINE FVSS(FVS,N,V,X,YS,Z,S,PHS,WS1,WS2,WS3,WS4,WS5,WS7,WS9)
        DIMENSION FVS(100,100)
        INTEGER V
        VS1=(X*SIN(PHS))/((X**2.)+(Z*COS(PHS)-YS*SIN(PHS))**2.)
        VS2=WS2
        VS3=WS3
        VS4=WS4
        VS5=WS5
        VS6=(Z-S*SIN(PHS))/((YS-S*COS(PHS))**2.+(Z-S*SIN(PHS))**2.)
        VS7=WS7
        VS8=(Z+S*SIN(PHS))/((YS+S*COS(PHS))**2.+(Z+S*SIN(PHS))**2.)
        VS9=WS9

        FVS(V,N)=VS1*(VS2/VS3-VS4/VS5)+(VS6*VS7)-(VS8*VS9)
```

```
      RETURN
      END
C
C     ************ SUBROUTINE FVP ****************
C     *                                          *
C     *** SIDEWASH COEFFICIENT- PORT WINGLET ***
C
      SUBROUTINE FVPP(FVP,N,V,X,YP,Z,S,PHP,WP1,WP2,WP3,WP4,WP5,WP7,WP9)
        DIMENSION FVP(100,100)
        INTEGER V
        VP1=(X*SIN(PHP))/((X**2.)+(Z*COS(PHP)-YP*SIN(PHP))**2.)
        VP2=WP2
        VP3=WP3
        VP4=WP4
        VP5=WP5
        VP6=(Z-S*SIN(PHP))/((YP-S*COS(PHP))**2.+(Z-S*SIN(PHP))**2.)
        VP7=WP7


        VP8=(Z+S*SIN(PHP))/((YP+S*COS(PHP))**2.+(Z+S*SIN(PHP))**2.)
        VP9=WP9

        FVP(V,N)=VP1*(VP2/VP3-VP4/VP5)+(VP6*VP7)-(VP8*VP9)
      RETURN
      END
```

1. Report No.	2. Government Accession No.	3. Recipient's Catalog No.
NASA TM-85815		

4. Title and Subtitle	5. Report Date
An Experimental and Theoretical Analysis of the Aerodynamic Characteristics of a Biplane-Winglet Configuration	June 1984
	6. Performing Organization Code: 505-43-43-01
7. Author(s): Peter D. Gall	8. Performing Organization Report No.
	10. Work Unit No.
9. Performing Organization Name and Address: NASA Langley Research Center, Hampton, Virginia 23665	11. Contract or Grant No.
	13. Type of Report and Period Covered: Technical Memorandum
12. Sponsoring Agency Name and Address: National Aeronautics and Space Administration, Washington, DC 20546	14. Sponsoring Agency Code

15. Supplementary Notes

Collateral publication of thesis submitted in partial fulfillment of the requirements for the Degree of Master of Science in Aerospace Engineering for the Pennsylvania State University.

16. Abstract

Improving the aerodynamic characteristics of an airplane with respect to maximizing lift and minimizing induced and parasite drag are of primary importance in designing lighter, faster, and more efficient aircraft. Previous research has shown that a properly designed biplane wing system can perform superiorly to an equivalent monoplane system with regard to maximizing the lift-to-drag ratio and efficiency factor. Biplanes offer several potential advantages over equivalent monoplanes, such as a 60-percent reduction in weight, greater structural integrity, and increased roll response. The purpose of this research is to examine, both theoretically and experimentally, the possibility of further improving the aerodynamic characteristics of the biplane configuration by adding winglets. Theoretical predictions were carried out utilizing vortex-lattice theory, which is a numerical method based on potential flow theory. Experimental data were obtained by testing a model in the Pennsylvania State University's subsonic wind tunnel at a Reynolds number of 510,000. The results showed that the addition of winglets improved the performance of the biplane with respect to increasing the lift-curve slope, increasing the maximum lift coefficient, increasing the efficiency factor, and decreasing the induced drag. A listing of the program is included in the Appendix.

17. Key Words (Suggested by Author(s))	18. Distribution Statement
Induced drag Induced velocity Biplane Winglet Vortex-lattice	UNCLASSIFIED - UNLIMITED STAR CATEGORY 05 - AERODYNAMICS

19. Security Classif. (of this report)	20. Security Classif. (of this page)	21. No. of Pages	22. Price
UNCLASSIFIED	UNCLASSIFIED	97	A05

For sale by the National Technical Information Service, Springfield, Virginia 22161